nature communications

Article

https://doi.org/10.1038/s41467-025-59571-y

The immune NIK1/RPL10/LIMYB signaling module regulates photosynthesis and translation under biotic and abiotic stresses.

Received: 19 March 2024

Accepted: 23 April 2025

Published online: 13 May 2025

Check for updates

Marco Aurélio Ferreira[1,2,7] ✉, Ruan M. Teixeira[1,2,7], Otávio J. B. Brustolini[1,3], Thainá F. F. Saia[2], James Jean-Baptiste[2], Nathalia G. A. Ribeiro[2], Sâmera S. Breves[2], Fellipe R. Sampaio[2], Eulálio G. D. Santos[1,2], Borys A. Leon[2], Celio C. Oliveira[4], Christiane E. M. Duarte[2,5], Lucas L. Lima[1], Leandro L. Oliveira[6], Humberto J. O. Ramos[1,2], Pedro A. B. Reis[1,2] & Elizabeth P. B. Fontes[1,2] ✉

Photosynthesis and translation are targets of metabolic control and development in plants, yet how stress signals coordinately regulate these opposing energy-producing and consuming processes remains enigmatic. Here, we unravel a growth control circuit that ties photosynthesis to translational control in response to biotic and abiotic signals. Our findings reveal that the L10-INTERACTING MYB DOMAIN-CONTAINING PROTEIN (LIMYB), a key player of the NUCLEAR SHUTTLE PROTEIN-INTERACTING KINASE 1 (NIK1)/RIBOSOMAL PROTEIN L10 (RPL10) antiviral signaling pathway, not only downregulates translation genes, but also represses photosynthesis-related genes and photosynthesis itself. LIMYB repressor activity, regulated by phosphorylation, is crucial for the decline in photosynthesis under stress. NIK1 activation by PAMPs or the phosphomimetic NIK1-T474D represses photosynthesis-related genes and photosynthesis in control but not in *limyb* lines. Furthermore, heat and osmotic stress also activate the NIK1/RPL10/LIMYB signaling circuit in wild type. These stresses induce NIK1 phosphorylation, but not marker gene repression, in *limyb*, indicating that LIMYB connects NIK1 activation to stress-mediated downregulation of translation- and photosynthesis-related genes. This coordinated repression via the NIK1/RPL10/LIMYB module may help plants adapt to changing environments.

Plants are constantly exposed to environmental changes that can impact their growth, including changes in temperature, water supply, and attacks by pathogens and insects. However, understanding how these environmental changes specifically influence plant growth control is a highly complex task. The existing knowledge about the underlying mechanisms is still fragmented and rudimentary, making it challenging to fully assemble the molecular puzzle that governs plant growth under stress conditions. In plants, stress conditions profoundly affect two crucial processes that promote cell growth, namely translation and photosynthesis[1–3]. In addition, the activation of defense responses to pathogens often provokes stunted growth[3]. Despite these observations, our understanding of the molecular mechanisms that connect abiotic and biotic stress signals with the coordinated regulation of photosynthesis and translation remains limited.

The energy for plant growth is obtained via respiration and photosynthesis. Photosynthesis not only directly provides substrates for

A full list of affiliations appears at the end of the paper. ✉e-mail: marco.a.ferreira@ufv.br; bbfontes@ufv.br

the ATP-generating mitochondrial reactions but also supplies carbon skeletons for allocation in protein synthesis. Any stress condition that interferes with energy and carbon balance in the photosynthetic cell is expected to affect translation[3]. Consequently, the photosynthesis rate correlates with carbon allocation to translation, polysome abundance, and translational regulatory processes, including the phosphorylation of ribosomal proteins (RP) and translation initiation factors[4]. While the impact of photosynthesis on translation has been established at some level, the molecular mechanisms underlying the coordinate regulation of these processes are still poorly understood.

As the most energy-consuming cellular process, translation is often tightly regulated under stress conditions. The NUCLEAR SHUTTLE PROTEIN (NSP)-INTERACTING KINASE 1 (NIK1)-mediated antiviral signaling has been described as a translational control mechanism associated with plant immunity[5–9]. NIK1 is a leucine-rich repeat receptor-like kinase (LRR-RLK) initially identified as a virulence target of the begomoviral NSP1[10,11] Upon viral infection or recognition of viral pathogen-associated molecular patterns (PAMPs; begomovirus-derived nucleic acids), NIK1 undergoes oligomerization with itself or a yet-to-be-identified viral pattern recognition receptor (PRR), resulting in phosphorylation at a critical threonine residue, position 474[12,13]. Activated NIK1 then mediates the phosphorylation of the ribosomal protein L10, redirecting RPL10 to the nucleus[14]. In the nucleus, phosphorylated RPL10 interacts with the transcriptional repressor L10-Interacting Myb domain-containing protein, LIMYB, resulting in the full repression of translational machinery-related genes, including RP genes and translational initiation and elongation factors[15]. Prolonged activation of NIK1 leads to suppression of global translation[15]. Begomovirus cannot escape this translational regulatory mechanism of plant cells; the viral mRNAs are not efficiently associated with polysomes and translated, compromising infection[15,16]. Viral NSP binds to the kinase domain of NIK1 to counteract this antiviral defense[10,12]. Therefore, the NIK1-mediated antiviral signaling is evolutionarily overcome by the viral suppressor NSP. Nevertheless, NIK1 antiviral signaling also cross-communicates with antibacterial immunity imposing relevant implications[17]. Firstly, under normal conditions, NIK1 interacts with the pattern recognition receptor (PRR) FLS2 and its coreceptor BAK1 to prevent autoimmunity and hence interference with growth. Secondly, NIK1 interaction modulates the formation of the PAMP (flagellin)-induced FLS2-BAK1 immune complex, thereby controlling the extent of PAMP-triggered immunity (PTI) activation that could otherwise impact growth. Finally, the activated immune complex FLS2-BAK1 phosphorylates NIK1 at the key threonine-474 residue initiating the transduction of an antiviral signal that ultimately results in global translation suppression. Therefore, bacterial infection may induce NIK1-dependent resistance against subsequent virus infections. The bacterial PAMP-induced activation of NIK1-mediated host translational suppression may also contribute to the stunted growth observed during immune responses.

Recent network-centric analyses of the LRR-based cell surface interaction network (CSILRR) have provided evidence suggesting that NIK1 may be one of the most influential LRR-RLKs as information spreaders[7,17–19]. Therefore, NIK1 may oligomerize with different stimulus-sensing receptors to control translation under adverse conditions. We tested this hypothesis using two different approaches. Firstly, we uncovered the transcriptional landscape resulting from NIK1 activation by performing a ChiP-seq on LIMYB-GFP seedlings. Our objective was to examine whether NIK1 activation is associated with cellular processes beyond translation, thus providing insights into potential broader functions of NIK1. Secondly, we monitored the NIK1 activation under different stimuli known to elicit shared responses. By subjecting the plant system to these stimuli, we aimed to evaluate the extent to which NIK1 activation could be modulated and synchronized across diverse signaling pathways. These experimental approaches were undertaken to deepen our understanding of NIK1's role in signal transduction and translation regulation, and to shed light on its potential interactions with other receptors and cellular processes.

Results

LIMYB represses the promoter activity and expression of photosynthetic apparatus-related genes, leading to photosynthesis inhibition

As a downstream component of the NIK1 antiviral signaling, LIMYB represses translational machinery-related genes, which accounts for the NIK1-mediated translational control mechanism[15]. To assess further the LIMYB regulon, we performed RNA-sequencing (RNA-seq) and chromatin immunoprecipitation sequencing (ChIP-seq) experiments on LIMYB-GFP-overexpressing seedlings (Supplementary Figs. 1a, b). Through the integration of RNA-seq and ChIP-seq data, we identified a set of differentially expressed genes that were directly regulated by LIMYB. RNA-seq was performed with Col-0, LIMYB32-L1, and LIMYB32-L3 RNA (Supplementary Figs. 1c, d). The LIMYB-induced transcriptome was represented by 1105 upregulated genes and 1246 downregulated genes, resulting in a total of 2351 differentially expressed (DE) genes (>2-fold change up or down, $P < 0.01$, Supplementary Figs. 1e, f). The top (ranked by false discovery rate [≤0.05]) significantly enriched GO term was structural constituents of ribosomes, supporting the role of LIMYB in repressing translation-related processes[15] (Supplementary Figs. 1e and 2a, b). The ChIP-seq analysis identified LIMYB binding peaks across the Arabidopsis genome, resulting in 6248 represented transcripts. By overlapping these transcripts with the RNA-seq results, we identified 204 upregulated and LIMYB-bound genes and a set of 156 downregulated and LIMYB-bound genes (Supplementary Figs. 2b, c). These overlapping genes constituted the core LIMYB up-regulon and down-regulon, respectively. The enriched down- and upregulated categories of genes within these regulons are described in Supplementary Tables 1 and 2. Notably, these regulons included several previously known LIMYB-directly regulated genes, such as ribosomal protein (RP) genes (*RPL18E*, *RPL28E*, *RPS13*A, *RPS25*, *RPL13*, *RPL4/L1)*, as well as newly identified LIMYB targets[15] (Supplementary Table 3).

Consistent with its role in translational control, the core LIMYB down-regulon exhibited significant enrichment of translation-related GO terms, including structural constituents of ribosomes and translation (Supplementary Fig. 2b and Supplementary Table 1). The RNA-seq and ChIP-seq results indicated that several translational regulatory genes (translational initiation and elongation factors) and RP genes were LIMYB-regulated targets (Supplementary Tables 3 and 4). De novo discovery of enriched motifs within the LIMYB binding peaks identified the MYB-related binding sites C[A/C/T]AA[A/C/G]C (E-value 3.0e-350) and AAGAA[A/G][A/C] (E-value 3.8e-252) and a conserved element [A/G]TATAT[A/G] (E-value 1.0e-0.97) as top-scoring motifs (Fig. 1a). To examine functional significance of this motifs as cis-regulatory elements for LIMYB assembly on promoters, we mapped the ChIP-seq peaks and RNA-seq hits to the loci of selected RP genes, and translational regulatory factors (Fig. 1b). The ChIP-seq peaks were mapped to these motifs on the promoter region of these LIMYB target genes. The corresponding transcripts were downregulated in the LIMYB-overexpressing lines, as shown by the RNA-seq hits and confirmed by RT-qPCR (Figs. 1b and Supplementary Fig. 2d–e). Additionally, a promoter transactivation assay demonstrated that a truncated version of the RPL18A promoter (pL18A, 325 bp) lacking the LIMYB binding sites at the -455 position (Supplementary Fig. 3a) was no longer downregulated by LIMYB in agroinoculated *Nicotiana. benthamiana* leaves (Fig.1c). The accumulation of LIMYB transgene in the transformed leaves was monitored by immunoblotting (Supplementary Fig. 3b). EMSA demonstrated that an E coli-produced and purified His-LIMYB protein (Supplementary Fig. 3c) directly bound to a 26-bp DNA fragment containing the CAAAAC sequence from the RPL18 promoter (Fig. 1d). The specificity of LIMYB binding to the CAAAAC site was confirmed as an excess of unlabeled CAAAAC-containing

https://doi.org/10.1038/s41467-025-59571-y

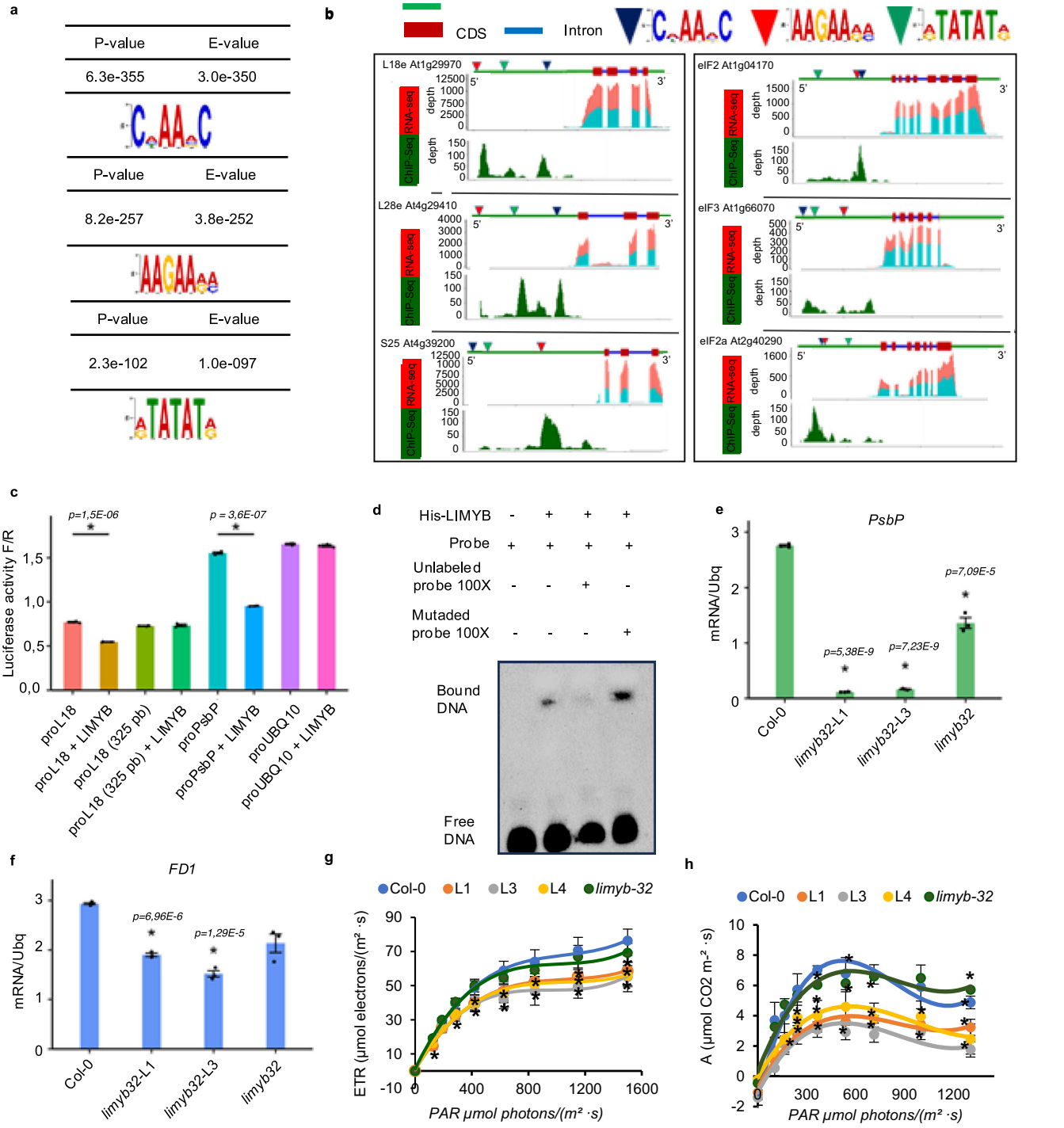

dsDNA, but not mutated dsDNA containing ATCGTG instead of CAAAAC, competed for binding. These findings, along with previous observation of LIMYB transcriptional repressor activity and binding to RP promoters, provided further evidence for the role of LIMYB as a transcriptional repressor[15]. These complementary experiments further confirmed that LIMYB represses translational machinery-related genes as previously demonstrated[15], validating our ChIP-seq data. These current data implicated the core LIMYB down-regulon as direct target genes of LIMYB; thereby, shifting the focus to the core LIMYB down-regulon for more detailed analysis.

Another significantly enriched GO term in the downregulated core was represented by photosynthesis-related genes, including genes involved in photosystem II assembly, light reaction, and photosynthetic electron transport (Supplementary Fig. 4a, b and Supplementary Table 5). Enriching photosynthesis-related genes in the LIMYB down-regulon raised the hypothesis that LIMYB coordinates the repression of translation and photosynthesis to balance carbon demand and allocation in response to biotic signals. Consistent with this hypothesis, responses to starvation-related GO terms were significantly enriched in the upregulated regulon (Supplementary Table 2). This hypothesis was further supported by subsequent experiments.

The expression of selected photosynthesis-related genes, including the subunit *PsbP* gene of the Photosystem II (PSII) Oxygen-Evolving Complex, the subunit *PsbR* of PSII, *FERREDOXIN* (*FD1*) involved in the electron transport chain (ETC), and *LHCB1* of the Light Harvesting Chlorophyll Protein Complex was confirmed to be repressed by *LIMYB* overexpression through RT-qPCR (Figs. 1e, f, Supplementary Fig 4c).

Fig. 1 | LIMYB represses the expression of photosynthetic apparatus-related genes and inhibits photosynthesis. a Top enriched motifs in the promoter region of LIMYB-regulated genes. The *p*-value was calculated using a statistical model based on log-likelihood ratios (LLRs) and adjusted for multiple testing using the Benjamini-Hochberg (BH) method. **b** LIMYB DNA-binding motifs are enriched in the promoter region of LIMYB downregulated genes. In the schematic representation, upstream promoter sequences are green, and coding regions are red. ChIP-seq peaks map to the promoter region, whereas the RNA-seq hits lay in the coding region. Abundance of RNA-sequencing hits in blue (LIMYB) and red (Col-0) shows the relative gene expression in Col-0 and LIMYB-overexpressing lines. **c** LIMYB represses the PsbP promoter. *N. benthamiana* leaves were agroinfiltrated with promoter fusions as shown and the 35S: LIMYB construct. After 48 h, luciferase activity was measured from total protein extracts from transformed leaves. An unrelated Ubiquitin promoter (UBQ) was used as a negative control. Results are mean values ± SE ($n = 6$). Asterisks indicate significant differences from the control line (two-tailed unpaired Student's *t*-test, $p < 0.05$). **d** LIMYB binds to the CAAAAC DNA binding motif on the RPL18 promoter by EMSA. A 26-bp-biotinylated CAAAAC-containing fragment was incubated with purified His-LIMYB, and the DNA-protein complex was resolved by SDS-PAGE. A 100-fold molar excess of unlabeled RPL18 26-bp dsDNA was used as a specific competitor, and a mutated 26-bp dsDNA containing ATCGTG as a nonspecific competitor. **e**, **f** The *PsbP* (subunit of the *PHSII-OEC*) and *FD1* (Ferredoxin) genes are repressed by LIMYB. The transcript levels were quantified by RT-qPCR in *LIMYB*-overexpressing (*limyb*-32-L1 and *limyb*-32-L3) lines and Col-0. Data are presented as mean ± SE from three independent replicates. Statistical significance was assessed using one-way analysis of variance (ANOVA), followed by Dunnett's post hoc test for multiple comparisons with the control group. Asterisks indicate significant differences from the control line ($p < 0.05$). **g** Electron transport rate (ETR) in *LIMYB*-overexpressing lines (*limyb*-32-L1, L3, L4), and *limyb* knockout line. PAR denotes Photosynthetically Active Radiation. **h** CO_2 assimilation rate (A) is reduced in *LIMYB*-overexpressing lines. For **g**, **h** data are mean ± SE ($n = 6$). Asterisks indicate significant differences from the control line (two-tailed unpaired Student's *t*-test, $p < 0.05$). Exact *p*-values in the Source Data file.

Furthermore, a firefly *LUCIFERASE* (fLUC) reporter construct containing a 2-kb 5′flanking region of the *PsbP* gene, which includes LIMYB binding sites, was used for transactivation assays with LIMYB in *N. benthamiana* leaves (Fig. 1c). The transient expression of LIMYB inhibited the *PsbP* promotor activity but not the UBQ promoter activity, which served as a control (Fig. 1c). As a newly-discovered LIMYB target, we used the AlphaFold3 to predict the interactions between RPL10-LIMYB complex and the −2000bp 5′flanking sequence of the *PsbP* gene (Supplementary Fig. 5). LIMYB assembled correctly on the *PsbP* promoter and interacted strongly with the sequences (in green) that are perfect match with the LIMYB DNA binding site (Fig. 1a). Finally, we showed that *LIMYB* overexpression inhibited the electron transport rate (ETR), which was accompanied with decreases in the photosynthetic rate (*A*), stomatal conductance (*gs*), transpiration rate (*E*), internal CO2 concentration (ci), quantum yield of PSII electron transport (ΦPSII) and water use efficiency (WUE) compared to the wild-type Col-0 (Figs. 1g, h, and Supplementary Fig. 6a–e). The simultaneous decrease in ETR, gas exchange parameters (A, gs, E and Ci), ΦPSII, and WUE in *LIMYB*-overexpressing lines suggests that the reduced photosynthetic activity may be due to a lower abundance of Photosystem II, I, ETC components rather than defects in CO_2 fixation or damages to the photosynthetic apparatus. Adjustments in the photosystem stoichiometry have been shown to affect the quantum efficiency of photosynthesis[20]. To address these hypotheses, we conducted a quantitative proteomic analysis to examine the abundance of specific PSII proteins and determined the sugar content in LIMYB-overexpressing lines. The proteomic data revealed significant changes in ribosomal protein and photosynthesis-related peptide abundance in the LIMYB-overexpressing lines x WT comparison, reflecting an 80% match with the RNA-seq analysis. Less abundant peptides are shown in Supplementary Table 6. Additionally, immunoblotting of specific PSII subunits demonstrated that the protein levels of PsbA, PsbD, PsbQ, PsbO1/O2 were lower in LIMYB-overexpressing lines compared to Col-0 (Supplementary Figs. 7a, b, c, d). These results correlated with the RNA-seq data (Supplementary Table 7). Not all down-regulated PSII components in the overexpressing lines are direct targets of LIMYB, as they do not appear in the intersection of RNA-seq and ChIP-seq data. This observation further supports the hypothesis regarding the stoichiometric adjustment of PSII components in the overexpressing lines. No significant differences in sugar accumulation were detected between control and overexpressing lines (Supplementary Fig. 7e, f).

Overall, these findings support the notion that LIMYB plays a role in coordinating the repression of translation (as previously shown[15]) and photosynthesis (as shown here), potentially to balance carbon demand and allocation under biotic signals. The regulation of translational machinery-related genes and translation by the NIK1/RPL10-LIMYB signaling module has been previously demonstrated[15]. The regulation of photosynthesis-related genes by LIMYB was demonstrated here through various experimental approaches, including gene expression analysis, transactivation assays, and measurement of photosynthetic parameters.

In addition to LIMYB-mediated reduced photosynthetic activity, the LIMYB-overexpressing lines displayed stunted growth under short or long-day light regimes (Supplementary Fig. 8a). Fresh weight, chlorophyll and carotenoids content, germination and root length were also lower in the LIMYB-overexpressing lines (LiMYB-32-L1 and LIMYB-32-L3) compared to the wild-type (Supplementary Figs. 8b, c, d, e). During the reproductive stage, however, no significant differences were observed among the genotypes (Supplementary Figs. 8f, g). Conversely, the photosynthetic function in *limyb* knockout lines did not significantly differ from the wild-type under normal conditions (Fig. 1g, h) consistent with their similar vegetative growth performance as shown here (Supplementary Fig. 8a) and previously[21].

We next examined whether the decreased photosynthesis in LIMYB-overexpressing lines was primarily associated with the LIMYB transcriptional activity or LIMYB-mediated suppression of global translation, which would have affected the expression of the photosynthetic genes. We have previously shown that the NIK1-mediated translational suppression is a delayed response, with a 30% reduction of translation observed only after 8-h of NIK1 activation in Arabidopsis seedlings[15]. Here, we showed that LIMYB represses the promoter activity of *the RPL18* marker gene (Fig. 1c) and induces a coordinated decrease in mRNA and protein (luciferase activity) levels after 3-h of the activated NIK1-T474D expression (Fig. 2a, b) or viral PAMP-mediated NIK1 activation (Fig. 2c, d). In contrast, LIMYB does not affect either the UBQ promoter activity or luciferase mRNA accumulation, which remains at normal levels throughout the experiment (Figs. 1c and 2e–g). However, it does promote a decrease in luciferase activity 8-h after NIK1 activation, indicating the late response of translational control (Fig. 2f–h). Notably, mRNA and luciferase activity under the control of the LIMYB target promoter RPL18 were simultaneously reduced as an early transcriptional response to NIK1 and LIMYB activation, and luciferase activity did not decline further during the translational suppression phase. These results indicate that the LIMYB's transcriptional repressor activity may account at least in part for the LIMYB-mediated control of photosynthesis. The early transcriptional response of LIMYB target genes, such as *RPL18*, to NIK1 activation leading to earlier reduced protein levels substantiates the notion that LIMYB may regulate photosynthesis by directly repressing the expression of photosynthesis-related genes. Therefore, the LIMYB's role in controlling photosynthesis may be primarily mediated through its early transcriptional repression activity rather than the late NIK1 circuit-mediated global translational suppression.

https://doi.org/10.1038/s41467-025-59571-y

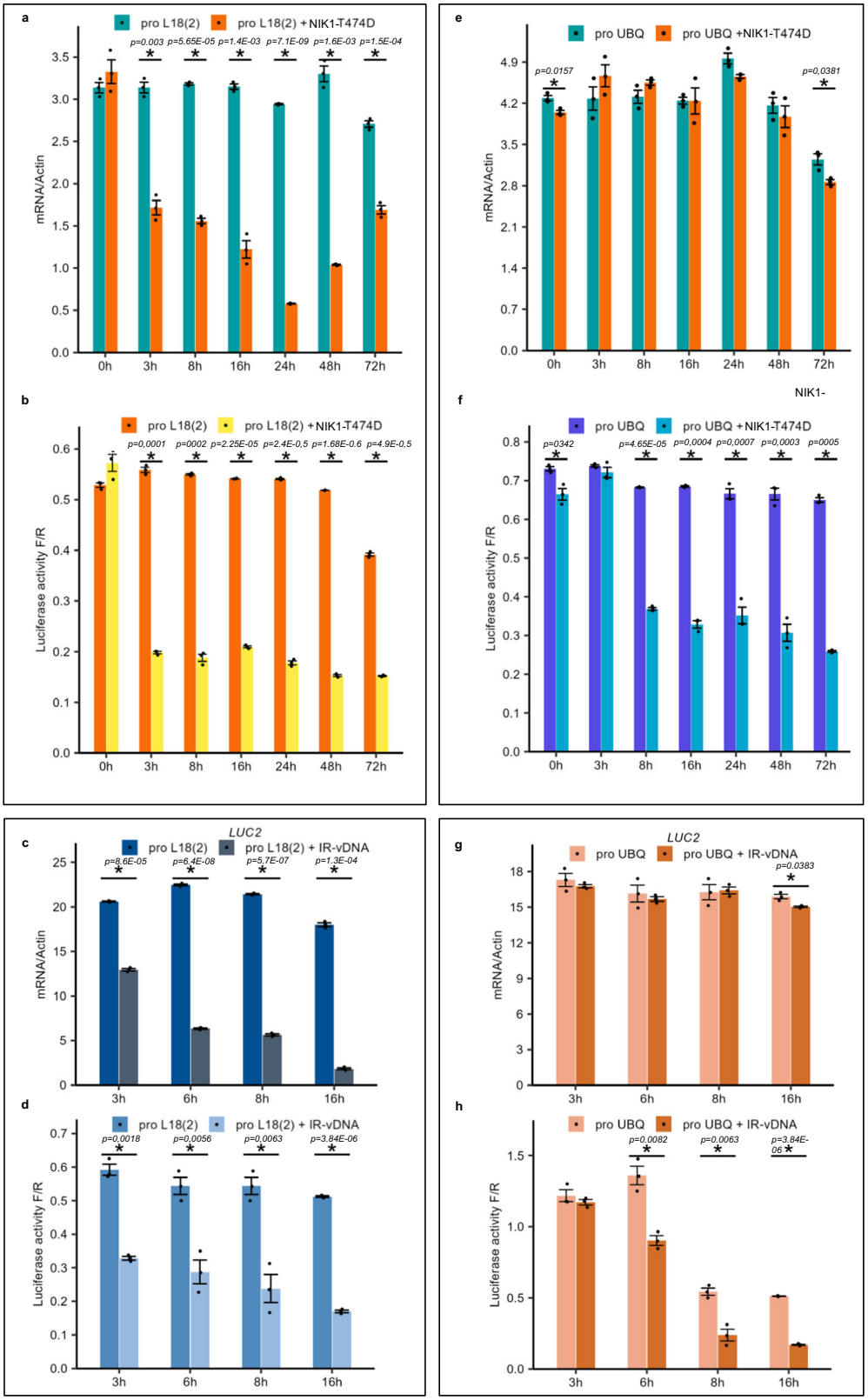

LIMYB-mediated repression of the photosynthetic activity is coupled to NIK1 activation

We also investigated the potential link between LIMYB-mediated control of photosynthesis and NIK1 activation. We first examined whether activation of NIK1 by viral PAMPs would lead to the repression of photosynthetic apparatus-related genes, like its effect on translation-related genes[13]. Treatment of NIK1-HA seedlings with RNA (InRNA) and DNA (InDNA) from begomovirus-infected, but not from mock-inoculated (UnRNA, UnDNA), Arabidopsis Col-0 lines induced rapid NIK1 phosphorylation (Fig. 3a) and resulted in *PsbP* repression (Fig. 3b). This repression of *PsbP* was less pronounced in the *nik1* and *nik2* single mutants and completely abolished in the *nik1nik2* double mutant. The expression levels of *PsbP* and *FD1* were significantly lower in transgenic lines expressing a constitutively activated NIK1 mutant

https://doi.org/10.1038/s41467-025-59571-y

Fig. 2 | LIMYB-mediated transcriptional repression of target genes causes an earlier reduction in protein levels that precedes the NIK1-mediated suppression of global translation. a The constitutively activated NIK1 mutant T474D represses the RPL18 promoter activity. Arabidopsis protoplasts were transformed with the proL18:luciferase construct alone or combined with the 35S:T474D construct. Time zero was considered 12 h after transfection. Transcript levels were determined by RT-qPCR (**a**) and luciferase activity was determined at different time points (**b**). **c**, **d** Time course of LIMYB-controlled mRNA accumulation (**c**) and luciferase activity under the control of RPL18 promoter (**d**). Protoplasts from *limyb* knockout lines co-transformed with 35S:LIMYB-GFP + proL18(2):Luciferase (proL18) or proUBQ:Luciferase (proUBQ) were treated with a viral PAMP (IR-vDNA; intergenic region from the component B of a begomovirus), and mRNA accumulation and luciferase activity were measured in the intervals of 3, 6, 8, and 16 h after the viral PAMP treatment. Time zero was considered 12 h after transfection. **e**, **f** NIK1-T474D does not affect the activity of the LIMYB non-target UBQ promoter. Arabidopsis protoplasts were transformed with the proUBQ:luciferase construct alone or with the 35S:T474D construct. Transcript levels were determined by RT-qPCR (**e**), and luciferase activity was determined at different time points (**f**). Time zero was considered 12 h after transfection. **g**, **h** LIMYB does not target the UBQ promoter but decreases luciferase activity (protein level) as a late response. Progression time of mRNA accumulation and luciferase activity under the control of the UBQ promoter after LIMYB expression. For **a**, **b**, **e**, **f**, the results are presented as mean values ± SD ($n = 6$) and for **c**, **d**, **g**, **h**, data are mean ± SD ($n = 3$). Asterisks indicate significant differences from the control line (two-tailed unpaired Student's *t*-test, $p < 0.05$). The experiments were repeated at least twice with similar results.

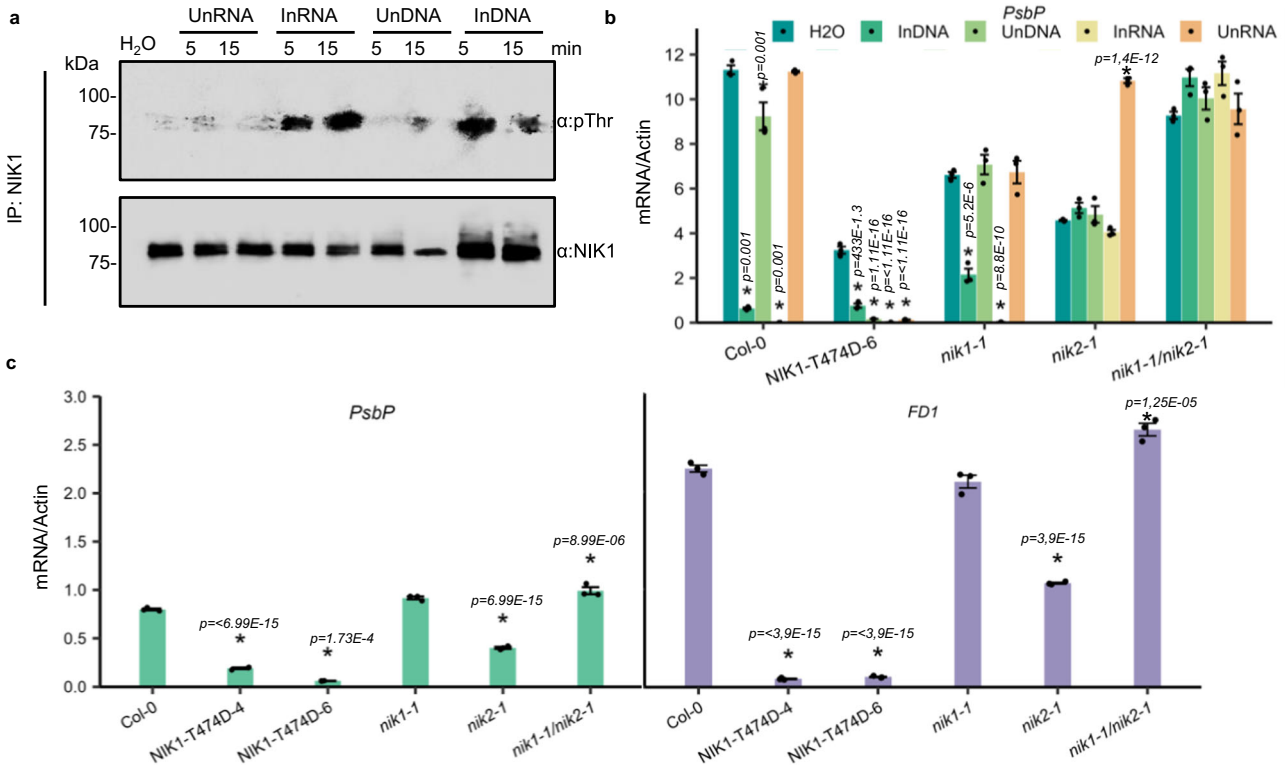

Fig. 3 | NIK1 activation by biotic signals represses the expression of photosynthetic apparatus-related genes. a NIK1 is rapidly phosphorylated by begomovirus-derived nuclei acids. NIK1-HA-expressing Arabidopsis seedlings were treated with RNA or DNA prepared from mock-inoculated (UnRNA and UnDNA) or begomovirus-infected (InRNA and InDNA) plants for the time indicated in the figure. NIK1 was immunoprecipitated with an α-NIK1 antibody and probed with an α-phospho-threonine antibody. **b** Viral PAMPs require NIK1 and/or NIK2 to repress the expression of the *PsbP* gene. Leaf discs of the indicated genotypes were treated with InRNA and InDNA, and PsbP transcript levels were quantified by RT-qPCR. NIK1-T474D-6 is a transgenic line that expresses the NIK1-T474D mutant. **c** Constitutive activation of NIK1 in T474D-expressing (T474D-4 and T474D-6) lines downregulates *PsbP* and *FD1*. Total RNA from the indicated genotypes and the transcript levels of the indicated genes were quantified by RT-qPCR. For (**b** and **c**) data are presented as mean ± SE from three independent replicates. Statistical significance was assessed using one-way analysis of variance (ANOVA), followed by Dunnett's post hoc test for multiple comparisons with the control group. Asterisks denote statistically significant differences from the control line at $p < 0.05$.

(NIK1-T474D) compared to Col-0, indicating that NIK1 signaling controls the expression of the photosynthesis-related genes (Fig. 3c). Expression of the phosphomimetic mutant NIK1-T474D has been previously demonstrated to sustain NIK1 activation, resulting in repression of translation machinery-related genes and suppression of global translation[15,16].

Consistent with the NIK1 activation-mediated repression of photosynthesis-related genes, independently transformed lines expressing NIK1-T474D displayed reduced ETR compared to the control line (Fig. 4a). This phenotype was accompanied with decreases in gas exchange parameters, including A, gs, E, Ci, ΦPSII, and WUE (Fig. 4b–g). Accordingly, T474D lines displayed a drastic, negative effect on growth (Supplementary Fig. 9a) and exhibited lower fresh weight, germination and root length compared to control lines (Supplementary Figs. 9b, c, d). The stronger growth defects of T474D-6 line compared to T474D-4 line may result from differing expression levels of the mutated NIK1 protein[15]. In contrast, the loss-of-NIK1/NIK2 function enhanced ETR and increased the gas exchange parameters. In addition, T474D expression in *limyb* mutant did not decrease ETR and photosynthetic activity or repress the expression of photosynthesis-related marker genes (Fig. 4a–h). These results establish a connection between NIK1 activation and LIMYB-mediated repression of photosynthesis-related genes, similar to the previously described control of translation-related genes mediated by the NIK1/RPL10/LIMYB signaling module[15].

https://doi.org/10.1038/s41467-025-59571-y

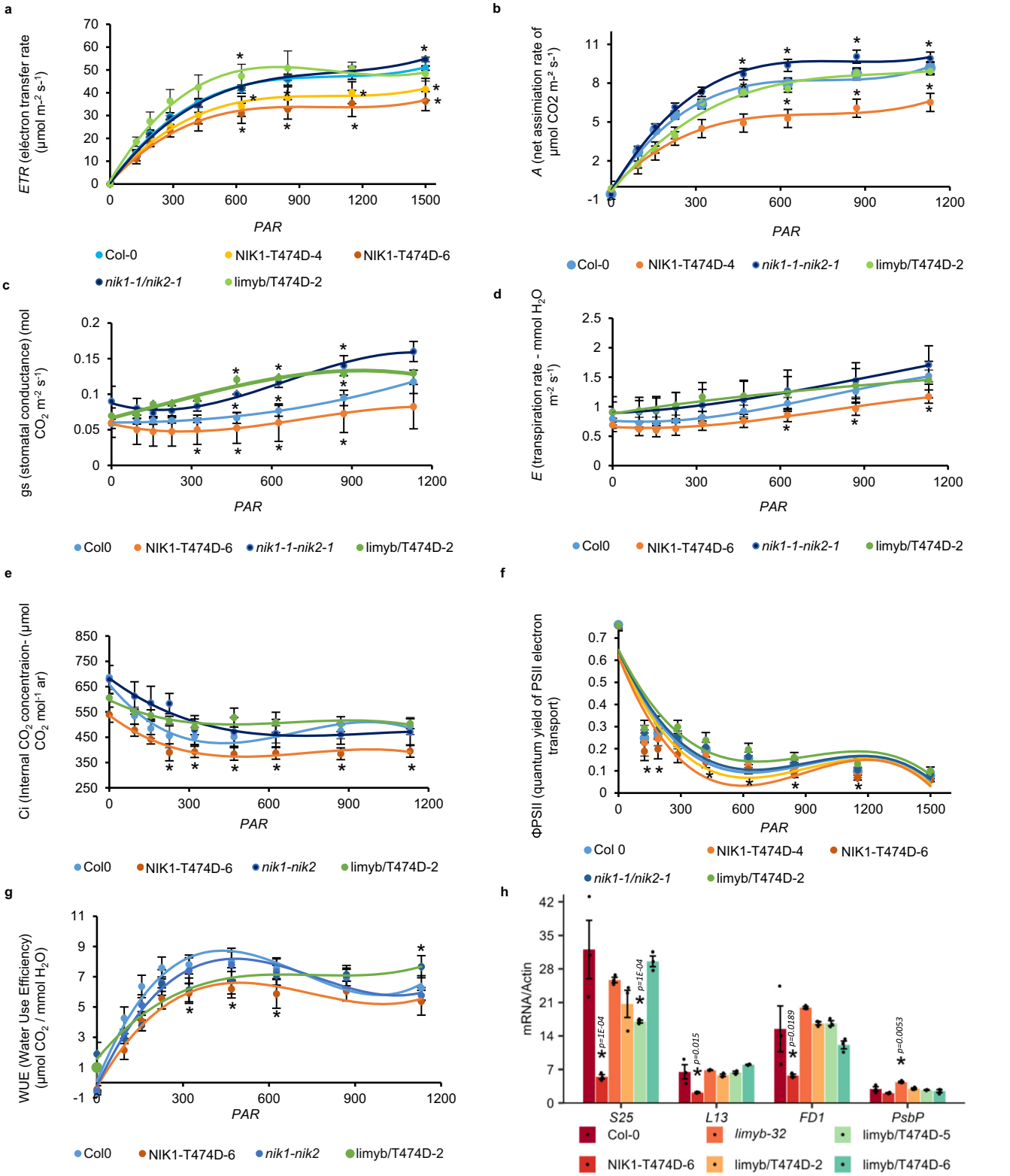

Fig. 4 | The LIMYB-mediated inhibition of photosynthesis depends on NIK1 activation. Leaf gas exchange parameters and photochemical processes were measured in expanded leaves from 30-days-old plants from the indicated genotypes. **a** electron transport rate (ETR), **b** net CO_2 assimilation rate (A), **c** stomatal conductance (gs), **d** transpiration rate (E), **e** the internal concentration of CO_2 (Ci), **f** quantum efficiency (ΦPSII), **g** water-use efficiency (WUE) The experiments were repeated at least twice with similar results. Bars (± SD) with an asterisk differ from each other by the two-tailed unpaired Student's t-test ($p < 0.05$), $n = 5$. **h** T474D requires the function of LIMYB to mediate photosynthesis-related gene repression. RNA were extracted from three *limyb* lines, ectopically expressing 35S::T474D, and the expression of photosynthesis-related genes was monitored by RT-qPCR. The experiments were repeated three times with similar results. Data are mean ± SE ($n = 6$). Asterisks indicate significant differences from the control line (two-tailed unpaired Student's *t*-test, $p < 0.05$). The exact *p*-values can be found in the Source Data file.

The promoter-repressing activity of LIMYB is regulated by NIK1-mediated phosphorylation

Although we showed that LIMYB represses the expression of photosynthesis-related genes and inhibits photosynthesis, the inactivation of *LIMYB* did not significantly alter the photosynthetic function under normal growth conditions (Figs. 1g, h, and Supplementary Fig. 6). Either a functionally redundant paralog replaces LIMYB in *limyb* knockouts, or LIMYB is activated specifically under biotic stress and is therefore not required under the standard conditions of the experiment. The first hypothesis is unlikely because the closest related member of the SAINT/MYB superfamily, HAI1-Interactor 1 (HIN1), has been shown to diverge functionally from LIMYB[21]. HIN1 acts as a plant-specific RNA-binding splicing regulator, is involved in osmotic stress response, interacts with serine-arginine-rich (SR) splicing factors, and increases the splicing efficiency of intron retention-prone stress-related genes. In contrast, LIMYB lacks detectable RNA binding activity[21], is dispersed evenly in the nucleoplasm[15], and functions as a transcriptional repressor that binds specific sites on the promotor region of target genes[15] (Fig. 1c, d). In addition, the HIN1 splicing function is regulated by phosphorylation at positions S357 and S389, which are not conserved in LIMYB primary structure[21]. Finally, we showed that the loss-of-*LIMYB* function barely affects growth, whereas *LIMYB* overexpression inhibits growth even under normal conditions (Supplementary Fig. 8), opposite phenotypes from the HUN1 transgenic lines[21]. Collectively, these data confirmed that LIMYB and HIN1 diverge functionally and may not complement each other. Therefore, we tested the second hypothesis for the weak phenotype of the *limyb* mutant under the normal experimental condition, based on the assumption that LIMYB function is activated under stress conditions, thereby not needed in the absence of biotic stimuli.

We first performed additional luciferase transactivation assays in viral PAMP-treated protoplasts to examine whether LIMYB was regulated by biotic stimuli (Supplementary Fig. 10). Expression of the constitutively activated NIK1-T474D mutant repressed the RPL18 promoter activity, but not the non-target UBQ promoter, in protoplasts expressing *LIMYB* but not in non-complemented *limyb* knockouts (Supplementary Fig. 10a, b). These results further confirmed the specificity of LIMYB for ChiPed promoters and that NIK1-mediated downregulation of target promoters requires the LIMYB function. Monitoring LIMYB-GFP ectopic expression in *limyb* protoplasts also confirmed that the *limyb* mutant was a true knockout (Supplementary Fig. 10b). Importantly, treatment of *LIMYB*-expressing protoplasts with the viral PAMP InRNA, but not UnRNA, further repressed RPL18 and PsbP promoters, indicating that LIMYB may indeed be regulated by biotic stimuli. We further examined this hypothesis with complementary approaches.

As a downstream component of the NIK1 phosphorylation cascade, we examined the status of LIMYB phosphorylation under biotic stimuli known to activate NIK1 (Fig. 5). Endogenous LIMYB immunoprecipitated by an anti-LIMYB antibody was probed with an anti-phosphoserine antibody after bacterial PAMP flg22 and viral PAMP InRNA treatments. Like the biotic stress-mediated phosphorylation of NIK1 and RPL10, RNA from begomovirus infected (InRNA), but not from mock-inoculated (UnRNA) Col-0 lines, induced endogenous LIMYB phosphorylation in Col-0 (Fig. 5a) and YFP-LIMYB phosphorylation in the overexpressing lines L1 and L3 (Supplementary Fig 10c). Likewise, the bacterial PAMP flg22 induced endogenous LIMYB (Fig. 5a) and YFP-LIMYB phosphorylation (Supplementary Fig 10d). Nevertheless, InRNA and flg22 did not induce LIMYB phosphorylation in the *nik1/nik2* double mutant, indicating that LIMYB phosphorylation by viral and bacterial PAMPs required the NIK1/NIK2 function (Fig. 5b, c). Endogenous LIMYB also required *NIK1/NIK2* function for displaying target promoter-repressing activity, as InRNA treatment elicited repression of RPL18 promoter activity in Col-0 (proL18) but not in *nik1/nik2* double mutant line (proL18 + *nik1/nik2*), a phenotype that may be linked to NIK1-mediated LIMYB phosphorylation (Fig. 5d).

These data are also consistent with recently published flg22-induced phosphoproteomic data, which showed that treatment with flg22 enhanced the phosphorylation signal in the LIMYB phosphosites at positions Ser157, Ser160, and Ser 161 (fdr<0.05)[22]. Based on these data, we mutated Ser157 to Ala, creating the LIMYB-S157A mutant, and the diphosphoserines 160 and 161 to Ala, creating the LIMYB-S160AS161A (Supplementary Fig. 11a) and assayed for viral PAMP-induced phosphorylation. Replacing the Ser157 with Ala slightly reduced the InRNA-induced phosphorylation in the S157A mutant, indicating that Ser157 is phosphorylated in response to NIK1 activation (Fig. 5e). The stability of the S157A mutant in protoplasts was further confirmed by immunoblotting (Supplementary Fig. 10b). Likewise, the replacement of Ser160 and Ser-161 with Ala did not alter the level of LIMYB phosphorylation mediated by NIK1-T474D expression (Supplementary Fig. S12a). The slight reduction of the phosphorylation signal in the S157A mutant and no alteration in S160A/S161A mutant indicated that other known flg22-induced phosphosites on LIMYB are also induced by a viral PAMP, maintaining an almost standard phosphorylation level in the mutant. Nevertheless, InRNA did not mediate translation and photosynthesis-related marker gene repression in *limyb* protoplast complemented with the LIMYB-S157A mutant (Fig. 5f). Likewise, flg22 did not induce translation and photosynthesis-related marker gene repression in *limyb* mutant stably expressing the S157A mutant, in contrast to Col-0 (Supplementary Fig. 12c). Also, the expression of the phosphomimetic mutant T474D did not repress translation and photosynthesis-related marker gene expression in *limyb* protoplast expressing the LIMYBS160A/S161A diphosphosite mutant (Supplementary Figs. 12b–d, e). Furthermore, InRNA repressed the activity of the LIMYB target RPL18 promoter in Col-0 protoplasts but not in *limyb* protoplast expressing S157A (Fig. 5d). Collectively, these results demonstrated that the promoter-repressing activity of LIMYB might be regulated by PAMP-induced phosphorylation at Ser157, Ser160, and Ser161[22]. The putative functional phosphosites are positioned between the MYB-SANT-like domains (R2 and CR3) and in proximity to the CR3 domain (Supplementary Fig. 11a, b). The molecular dynamics simulation-equilibrated models and subsequent structural comparison analysis for phospho and non-phospho-LIMYB suggest that phosphorylation at either Ser157 or Ser160/Ser161 residues promoted significant structural alterations in the positioning of the DNA major groove-binding helix at the CR3 domain (Supplementary Fig. 11c, d, Supplementary video), which corroborates with the consistent hydrogen bonds predicted with the positive residues of the domain (Supplementary Fig. 11e). The proximity of the functional phosphosites to the DNA interface and the decreased linker polarity in the likely phospho-null mutation-induced conformational changes may explain the lack of transcriptional repressing activity of either LIMYB mutants.

NIK1 may serve as a coreceptor for different biotic stress-sensing receptors

As a member of the subfamily II of LRR-RLKs containing predominantly coreceptors of stimulus-sensing transmembrane receptors, NIK1 may be a signal relay unit from different sensing receptors[23,24]. Accordingly, NIK1 has been shown to interact with several receptor-like kinases and may be one of the most influential information spreaders from the cell surface[17,19]. In addition, we have previously shown that NIK1 is phosphorylated by the bacterial PAMP-induced FLS2-BAK1 immune complex activating the NIK1/RPL10/LIMYB signaling module for translation control. In contrast, we showed here that viral PAMPs can activate NIK1 and induce subsequent RPL10 phosphorylation independently of FLS2/BAK1 for NIK1, consistent with the argument that NIK1 may serve as a

https://doi.org/10.1038/s41467-025-59571-y

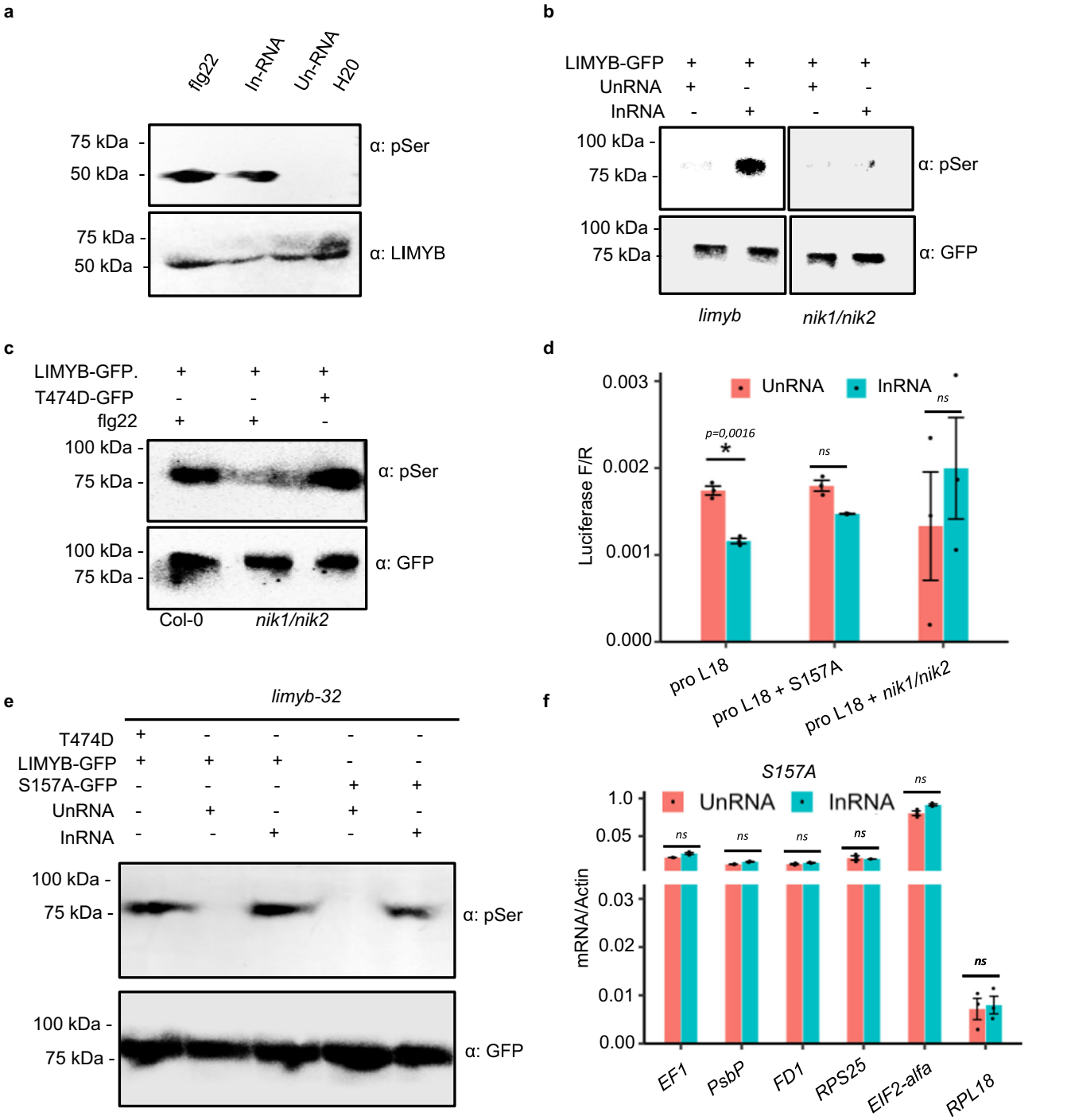

Fig. 5 | Biotic stimuli induce LIMYB phosphorylation via NIK1 activation. a The bacterial PAMP, flg22, and viral PAMP, InRNA, induce phosphorylation of endogenous LIMYB. Col-0 seedlings were incubated with RNA prepared from begomovirus-infected leaves (InRNA), mock-inoculated leaves (UnRNA), H_2O, and 100 mM flg22 for 3 h. LIMYB was immunoprecipitated from total protein extracts with an anti-LIMYB polyclonal antibody and immunoblotted with α-phosphoserine (α-pSer) (top) and α-LIMYB (bottom) antibodies. **b** Viral PAMP-induced LIMYB phosphorylation requires the *NIK1/NIK2* function. *limyb* and *nik1/nik2* protoplasts transfected with LIMYB-GFP were treated with InRNA or UnRNA, and the immunoprecipitated LIMYB-GFP was probed with an α-phosphoserine (α-pSer) antibody. **c** Flg22-induced phosphorylation of LIMYB requires the *NIK1/NIK2* function. Col-0 and *nik1/nik2* protoplasts transfected with LIMYB-GFP were treated with flg22. Half of the immunoprecipitated LIMYB was fractionated by SDS-PAGE and immunoblotted with an α-phosphoserine (α-pSer) antibody, and the other half with an α-GFP antibody. **d** LIMYB-S157A does not mediate the repression of the RPL18 promoter in the presence of InRNA. Col-0 protoplasts, LIMYB-S157A-expressing *limyb* protoplasts, and *nik1nik2* protoplasts were transfected with plasmids carrying the RPL13 promoter fused to luciferase and treated with UnRNA or InRNA. After 16 h, luciferase activity was measured from total protein extracts of transfected protoplasts. Data are mean values ± SD ($n = 3$) (two-tailed unpaired Student's *t*-test, $^*p < 0.01$, ns = not significant). **e** Ser157 is a possible phosphorylation site on LIMYB. The *limyb* protoplasts transfected with LIMYB-GFP or LIMYB-S157A-GFP were treated with InRNA or UnRNA and protein phosphorylation was assayed by immunoblotting immunoprecipitated GFP fusions with anti-phosphoserine antibody. **f** UnRNA fails to cause downregulation of NIK1 signaling-associated marker genes in LIMYB-S157A-expressing *limyb* protoplasts. RNA was extracted from UnRNA and InRNA-treated protoplasts, and transcript accumulation was determined by RT-qPCR. Results are mean values ± SD ($n = 3$) (two-tailed unpaired Student's *t*-test, $^*p < 0.01$, ns = not significant). All the above experiments were repeated at least twice with similar results.

https://doi.org/10.1038/s41467-025-59571-y

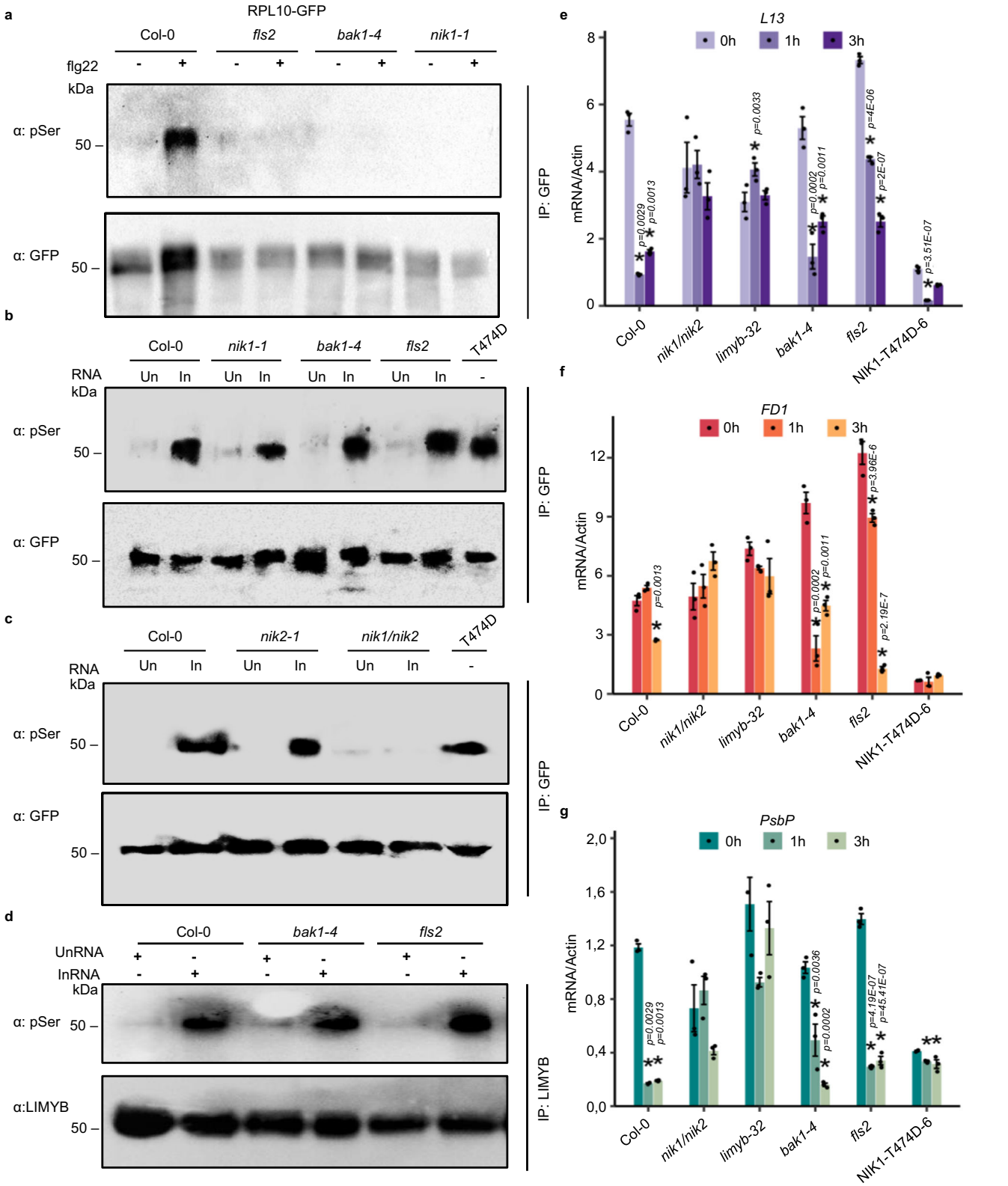

coreceptor from different receptors (Fig. 6). In this experiment, to detect the NIK1 antiviral signaling activation, we monitored the phosphorylation of the downstream components RPL10 and LIMYB by probing immunoprecipitated RPL10 and LIMYB with an anti-phosphoserine antibody. We also monitored LIMYB-mediated repression of the marker genes induced by viral PAMPs in *flg22* and *bak1* mutants. While the bacterial PAMP flg22 requires the receptor FLS2 and coreceptor BAK1 to induce the NIK1-mediated phosphorylation of the downstream component RPL10[17] (Fig. 6a), viral PAMP induced RPL10 and LIMYB phosphorylation and repression of marker genes in Col-0 but also in *fls2* and *bak1* knockout lines (Figs. 6b–d, e, f, g) and not in *nik1nik2* line (Fig. 6c). Collectively, these results indicated that viral PAMP might require a yet-to-be-identified viral PAMP-sensing receptor for NIK1 signaling activation.

Fig. 6 | Viral PAMPs require NIK1/NIK2, but not FLS2 and BAK1, to activate the RPL10/LIMYB signaling module. a The bacterial PAMP flg22 requires BAK1 and FLS2 to induce RPL10 phosphorylation. Arabidopsis protoplasts prepared from the indicated genotypes were transformed with 35S:RPL10-GFP. After 12-h for RPL10-GFP expression, the protoplasts were treated with PAMPs. Immunoprecipitated RPL10-GFP by an α-GFP antibody was probed with an α-phosphoserine antibody. The experiments were repeated at least three times with similar results. **b**, **c** RNA from infected plants requires NIK1/NIK2, but not FLS2 and BAK1, to mediate RPL10 phosphorylation. RNA prepared from mock-inoculated (Un) or begomovirus-infected (In) plants was used to activate NIK1 signaling. NIK1-T474D served as a positive control. Half of the immunoprecipitated RPL10-GFP from total protein extracts was fractionated by SDS-PAGE and immunoblotted with an α-phosphoserine (α-pSer) antibody and the other half was immunoblotted with an α-GFP antibody. **d** Viral PAMP induces LIMYB phosphorylation independent on BAK1 and FLS2. Seedlings from the indicated genotypes were treated with viral PAMPs for 30 min. LIMYB was immunoprecipitated with α-LIMYB antibody and probed with an α-phosphoserine antibody. **e**–**g** Viral PAMP activates NIK1 signaling and mediates repression of the indicated marker genes. Seedlings of the indicated genotypes were treated with viral PAMP InRNA for 1 h and 3 h and transcript accumulation was determined by RT-qPCR, using actin as an endogenous control for normalization. Data are presented as mean ± SE from three independent replicates. Statistical significance was assessed using one-way analysis of variance (ANOVA), followed by Dunnett's post hoc test for multiple comparisons with the control group. Asterisks indicate significant differences at $p < 0.05$.

The NIK1/RPL10/LIMYB signaling module is activated under abiotic stress conditions

As NIK1 may interact with different stimulus-sensing receptors, we investigated whether the NIK1/RPL10/LIMYB signaling module would function as a molecular link for the coordinate suppression of photosynthesis and translation under abiotic stress conditions. To test this hypothesis, we subjected Arabidopsis Col-0, *nik1*, *nik2*, and *nik1nik2* lines to different stress conditions and monitored the activation of the NIK1 signaling pathway. Initially, we examined high temperature because analyses of published heat transcriptional profiles demonstrated that the translation-related and photosynthesis-related genes (described in Supplementary Tables 3, 4, 5) were significantly and progressively downregulated by heat in a time- and heat intensity-dependent manner (Supplementary Fig. 13a). As an early response, heat (38°C) promoted endogenous NIK1 phosphorylation 10 min after treatment in Col-0 and *nik2* lines but not in *nik1* and *nik1nik2* mutants, confirming they were true NIK1 knockouts (Fig. 7a). As expected, T474D was constitutively phosphorylated at Ser residues. NIK1-HA also underwent phosphorylation under heat, indicating that the fusion protein was functional (Fig. 7b). We also monitored the effectiveness of the heat treatment by measuring *HSP70* induction (Supplementary Fig. 14a). Heat treatment also promotes phosphorylation of the downstream component RPL10-GFP as early as 30 min after treatment (Fig. 7c) and LIMYB-GFP (Fig. 7d), endogenous LIMYB (Fig. 7e) followed by repression of photosynthesis-related marker genes *PsbP* and *FD1* in Col-0, but not in *nik1/nik2* knockouts (Fig. 7f). Likewise, heat treatment promoted the repression of RP genes in control lines but not in the *nik1nik2* double mutant (Fig. 7g). In addition to *HSP70*, we included as an additional control, the *UBQ10* gene, a *LIMYB* non target gene, which consistently was not downregulated by heat (Supplementary Fig 14b). Expression of the phosphomimetic NIK1-T474D, used as a positive control, also induced phosphorylation of endogenous LIMYB, indicating that NIK1 activation is a trigger for LIMYB phosphorylation (Fig. 7e). Loss-of-*LIMYB* function did not prevent the rapid heat stress-induced phosphorylation of NIK1 (Fig. 7h) but impaired the later repression of marker gene expression in the *limyb* mutant (Fig. 7i). We also showed that moderate heat stress at 27 °C activated the NIK1 signaling, as it induced repression of the marker genes (Supplementary Figs. 13b, c, d) but not an unrelated gene, which was not a target of the RPL10/LIMYB module (Supplementary Fig 13e). Collectively, these data indicate that LIMYB couples the stress-induced NIK1 activation to translation and photosynthesis inhibition and may indicate that heat treatment activates the NIK1/RPL10/LIMYB signaling module to coordinate translation and photosynthesis during stress conditions.

We also examined the activation of the NIK1 signal transduction by osmotic stress, which inhibits growth (Fig. 8). The effectiveness of the osmotic stress treatment was confirmed by the induction of the drought-responsive marker gene *RAB18* 3-h and 24-h after treatment in all genotypes (Supplementary Fig. 14c). The osmotic stress inducer PEG mediated NIK1-HA phosphorylation (Fig. 8a), leading to RPL10-GFP phosphorylation (Fig. 8b), followed by repression of NIK1 activation-associated marker genes in Col-0, *nik1*, and *nik2*, but not in the *nik1nik2* double mutant (Fig. 8c, d). Furthermore, osmotic stress induced NIK1 phosphorylation, but not the repression of the NIK1 signaling-associated marker genes, in *limyb* knockout lines (Fig. 8e, f, g), suggesting that osmotic stress-mediated NIK1 activation requires LIMYB function to repress the expression of photosynthesis and translation-related genes. Therefore, the NIK1/RPL10/LIMYB regulatory circuit is activated by different biotic and abiotic signals, further supporting a role for the NIK1 signaling pathway in coordinating translation and photosynthesis under stress conditions.

The coordination of photosynthesis and translation allows organisms to maintain a balance between the production of chemical energy with its utilization in energy-consuming processes, particularly under stressful conditions that impact the primary metabolism of plant cells. This balance ensures efficient resource allocation and helps prevent detrimental effects such as oxidative stress. While inhibition of photosynthesis and translation negatively affects growth, as observed in transgenic lines ectopically expressing the gain-of-function NIK1-T474D mutant, any mechanism that mitigates the accumulation of oxidative stress is likely to confer a certain degree of stress tolerance. We addressed this issue by exposing the T474D lines and the loss-of-function mutants to a water deficit regime. The Col-0, *nik1-1*, *nik2-1*, *nik1/nik2* double mutant, *limyb-32*, and NIK1-T474D-6 lines were grown in soil for 30 days and subjected to drought by suspending irrigation until reaching the soil relative water content ~40%, followed by rehydration to 100% of field capacity (Supplementary Fig. 15). After rehydration, the T474D lines exhibited a significantly higher survival rate compared to the wild-type line, whereas the *limyb-32* and *nik1/nik2* mutants displayed a lower survival rate than the wild-type (Supplementary Figs. 15a, b). Throughout the water deprivation period, the T474D lines maintained higher levels of leaf relative water content, while the *nik1/nik2* and *limyb-32* mutants displayed a lower water retention capacity than the wild-type (Supplementary Fig. 15c). These results suggest that constitutive activation of NIK1 prevents stress build-up in response to water deprivation. This phenotype was associated with the activation of the NIK1/RPL10/LIMYB signaling module, as the loss of LIMYB and NIK1/NIK2 function compromised drought tolerance and increased susceptibility to water dehydration in the mutants.

Discussion

All organisms must perceive and respond to changing growth conditions and environmental stimuli. During acute adverse conditions, including heat shock, osmotic stress, and pathogen attack, the induced changes in energy-consuming cellular processes must be coordinated with the rate of energy-producing metabolic processes to prevent excessive stress built up and ensure cell survival. In-plant cells, photosynthesis, a chemical energy-producing process, needs to be effectively coordinated with translation, the most energy-consuming process, under stress conditions. However, the direct connections

https://doi.org/10.1038/s41467-025-59571-y

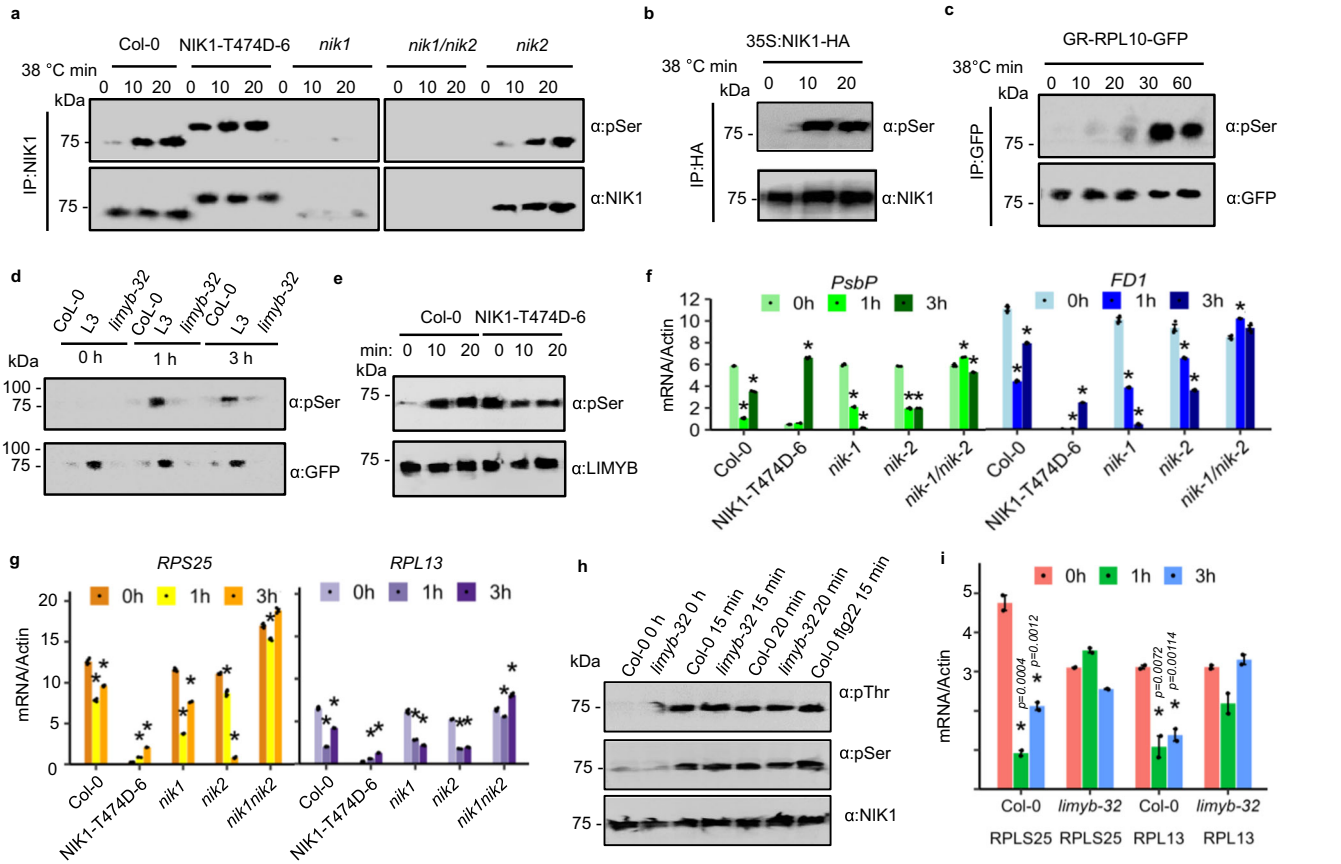

Fig. 7 | High temperature activates NIK1 antiviral signaling. a Rapid NIK1 phosphorylation induced by heat stress. Twenty-eight days-old plants were subjected to 38 °C for 0 to 3 h. NIK1 was immunoprecipitated from proteins extracts with an α-NIK1 antibody and probed with α-phosphoserine (p-Ser) and α-NIK1 antibodies. **b** NIK1-HA is correctly phosphorylated in response to heat. NIK1-HA-expressing lines were subjected to heat stress as in A. NIK1-HA was immunoprecipitated with an α-HA antibody and probed with α-pSer and α-NIK1 antibodies. **c** Heat stress mediates RPL10 phosphorylation. RPL10-GFP-overexpressing lines were heat-treated, and immunoprecipitated RPL10-GFP was probed with α-pSer and α-GFP antibodies. **d** Heat stress mediates LIMYB phosphorylation. YFP-LIMYB-expressing lines were heat treated for 1 h and 3 h. Immunoprecipitated LIMYB was probed with α-pSer. **e** Heat stress induces phosphorylation of endogenous LIMYB. Col-0 and T474D-expressing lines were heat-treated for the indicated time, LYMIB was immunoprecipitated with anti-LIMYB and probed with α-pSer. A T474D-expressing line is a positive control. **f** Heat stress represses *PsbP* and *FD1* genes in a NIK1- or NIK2-dependent manner. Plants were heat-treated for 1-h and 3-h and gene expression was analyzed by qRT-PCR. Data are shown as the mean ± SE ($n = 3$). Asterisks indicate statistically significant differences to the untreated sample (one way ANOVA, multiple comparisons, Dunnett's test $p < 0.05$). **g** High temperature suppresses ribosomal protein gene expression. RT-qPCR data are shown as the mean ± SE ($n = 3$). Asterisks indicate statistically significant differences to the untreated sample (one way ANOVA, multiple comparisons, Dunnett's test $p < 0.05$). For **f**, **g** Exact *p*-values in the Source Data file. **h** Heat stress induces rapid NIK1 phosphorylation in the *limyb* knockout line. NIK1 was immunoprecipitated with α-NIK and immunoblotted with α-phosphothreonine, α-phosphoserine, and α-NIK antibodies. **i** Heat stress does not induce repression of NIK1 signaling pathway-associated marker genes in *limyb*-32 mutant. The expression of the marker genes *RPL25* and *RPL13* was examined by RT-qPCR, 1-h, and 3-h post-treatment. Data are shown as the mean ± SE ($n = 3$). Asterisks indicate differences from the untreated sample (one way ANOVA, multiple comparisons, Dunnett's test $p < 0.05$). All the above experiments were repeated at least three times with similar results.

between these two crucial cellular processes have not been thoroughly investigated. We described a growth-controlling NIK1/RPL10/LIMYB signaling module that ties the photosynthetic function to translational control in response to biotic and abiotic signals. First, we showed that LIMYB binds in vivo to and inhibits the activity of photosynthesis-related promoters, leading to the repression of these target genes, similar to the translation-related target genes, as demonstrated previously[15]. Then, we demonstrated that the LIMYB-mediated repression of the photosynthesis-related genes led to a decrease in photosynthesis in a process that required the *NIK1/NIK2* function. We also showed that the stress-induced NIK1 phosphorylation mediated LIMYB phosphorylation, controlling the promoter-repressing activity of LIMYB in control lines but not in the *nik1/nik2* double mutant. Furthermore, the phosphomimetic, constitutively activated NIK1 mutant, NIK1-T474D, inhibited photosynthesis in control lines but not in the *limyb* mutant line. Both biotic and abiotic stimuli induced rapid NIK1 phosphorylation, followed by RPL10 and LIMYB phosphorylation, resulting in repression of the NIK1 signaling-associated marker genes in control lines but not in *limyb* knockout line. Collectively, these results demonstrated that LIMYB serves as a crucial link between biotic and abiotic-induced NIK1 activation and the repression of photosynthesis- and translation-related genes. The stress-induced LIMYB-mediated repression of these genes ensures the coordinated suppression of photosynthesis and translation. This coordination likely contributes to balance carbon fixation and allocation, preventing the occurrence of excessive oxidative stress. Therefore, the stress-induced repression of photosynthesis and translation, orchestrated by the NIK1/RPL10/LIMYB signaling module, plays a role in growth control in response to changing environmental conditions.

Compelling evidence in the literature indicates that the activation site of NIK1 signaling is the Thr-474 residue located within the kinase activation loop. This site, NIK1-T474, occupies a conserved position similar to the activation sites of BAK1 and SERK1, suggesting a similar activation mechanism among members of the LRR-RLK

https://doi.org/10.1038/s41467-025-59571-y

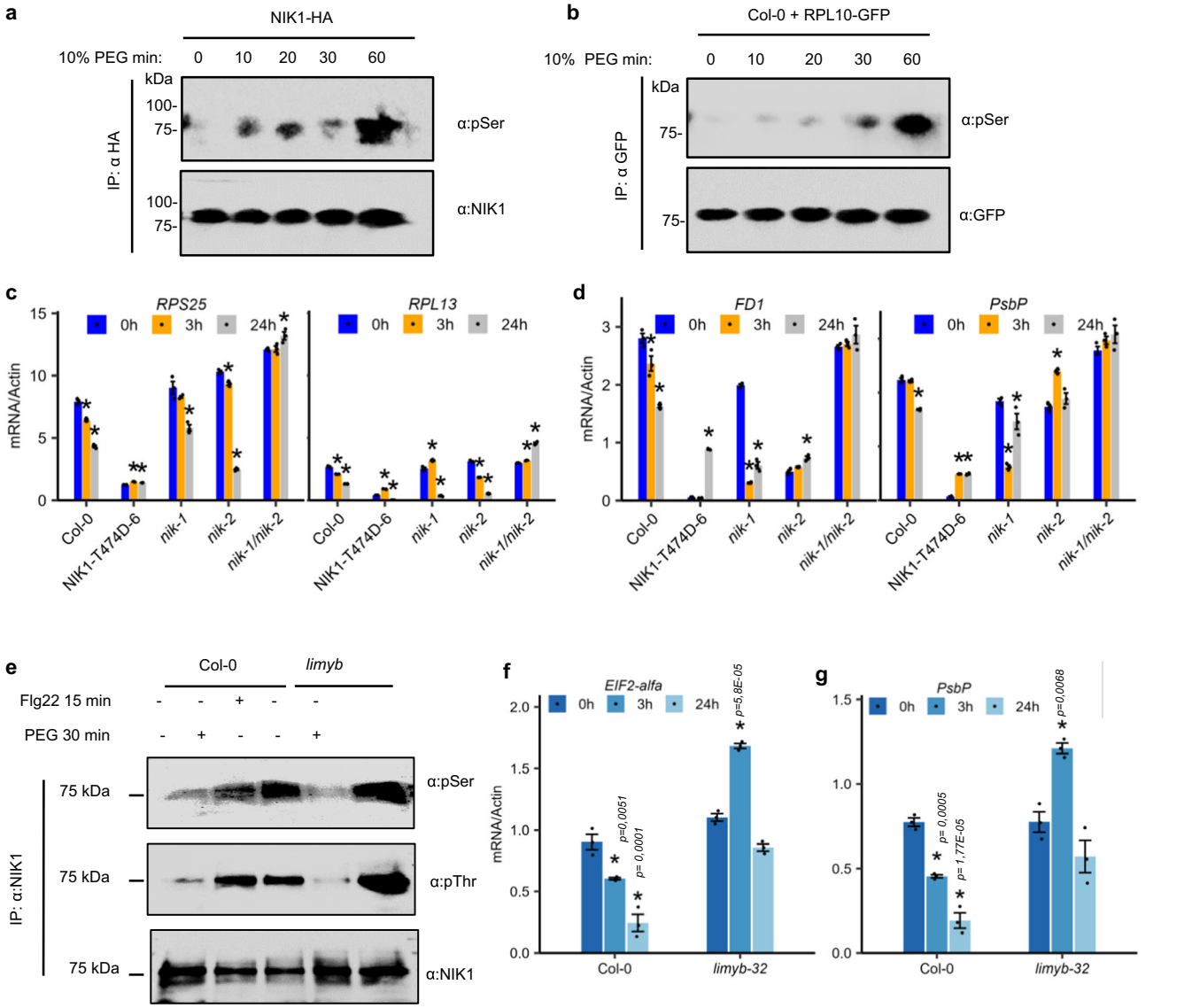

Fig. 8 | The osmotic signal triggers the NIK1 antiviral signaling activation. **a** NIK1 is phosphorylated under osmotic stress. NIK1-HA-expressing seedlings were treated with 10% PEG for the indicated intervals. The NIK1 phosphorylation was monitored by probing immunoprecipitated NIK1-HA with an α-pSer antibody. Immunoprecipitated NIK1-HA was probed with α-NIK1. **b** Osmotic stress induces RPL10 phosphorylation. Osmotic stress was induced in RPL10-GFP-expressing Arabidopsis seedlings, and then RPL10 phosphorylation was monitored by immunoblotting immunoprecipitated RPL10-GFP with an α-pSer antibody. **c** Osmotic stress-mediated repression of RP genes requires the function of NIK1 and/or NIK2. *RPS25* and *RPL13* expression was quantified by RT-qPCR 3-h and 24-h after PEG treatment in the indicated genotypes. A T474D-overexpressing line was used as a positive control. **d** Osmotic stress suppresses the photosynthetic genes *PsbP* and *FD1* in Col-0 but not in *nik1nik2* double knockouts. Transcript accumulation of *PsbP* and *FD1* was determined by RT-qPCR 3 h and 24 h after PEG treatment. **e** Osmotic stress induces NIK1 phosphorylation in the *limyb-32* knockout line. NIK1 was immunoprecipitated with an α-NIK antibody and probed with an α-phosphothreonine antibody and an α-phosphoserine antibody to monitor phosphorylation and with α-NIK antibody to visualize the immunoprecipitated NIK1. **f**, **g** Osmotic stress does not induce repression of NIK1 signaling pathway-associated marker genes in *limyb*-32 mutant. The expression of the marker genes was examined by RT-qPCR, at the time indicated in the Figure. For **c**, **d**, **f**, and **g** data are shown as the mean ± SE ($n = 3$). Asterisks indicate statistically significant differences from the untreated sample (one way ANOVA, multiple comparisons, Dunnett's test $p < 0.05$). For **c** the exact *p*-values can be found in the Source Data file. For **d** *p*-values: *FD1*, Col-0 (3 h): 0.0255; Col-0 (24 h): 0.0001; NIK1- T474D-6 (24 h): 1E-11; *nik-1*(3 h): 1.03E-07; *nik-1*(24 h): 3.32E-07; *nik-2* (24 h): 0.0010; *p*-value, *PsbB*, Col-0 (24 h): 5.2E-06; NIK1- T474D-6 (3 h): 2.41E-08; NIK1- T474D-6 (24 h): 2.46E-08; *nik-1*(3 h): 0.0001; *nik-1*(24 h): 0.0462; *nik-2* (3 h): 0.0008). For **f**, **g** *p*-values are shown in the Figure. The above experiments were repeated at least twice with similar results.

subfamily II[25,26]. Like BAK1 and SERK1 activation sites, substituting NIK1-Thr-474 with alanine significantly reduces in vitro autophosphorylation of the NIK1 T474A kinase mutant produced in E. coli as a GST-fused protein[12]. Consequently, this mutant loses its ability to promote phosphorylation and translocation of the downstream component RPL10 to the nucleus. As a result, the phosphonull mutant T474A fails to restore the antiviral function and antibacterial immunity repressing activity of NIK1 when expressed in the *nik1* knockout lines, as observed in an in vivo complementation assay[12,17]. In contrast, previous studies have demonstrated that substituting Thr-474 with Aspartate (T474D) leads to the constitutive activation of NIK-mediated defenses in Arabidopsis and tomato plants[15,16]. Furthermore, the gain-of-function mutant T474D can sustain NIK1 phosphorylation at additional sites and induce RPL10 and LIMYB phosphorylation even without stimuli, confirming that phosphorylation of Thr-474 is the crucial event triggering kinase activation (Figs. 5, and 6b, c). Supporting these data, a recent phosphoproteomic analysis discovered that Flg22 induces in vivo

phosphorylation of NIK1/NIK2 at Thr-474, as well as Ser-465 and Ser-615[22]. Accordingly, we have shown previously that flg22-mediated NIK1 phosphorylation relies on BAK1 activation, which phosphorylates NIK1 at the crucial Thr-474 residue in vitro[17].

Moreover, we have previously shown that overexpression of T474D in Arabidopsis and tomato plants results in downregulating translation-related genes and suppressing global translation in a LIMYB-dependent manner[15,16]. Similarly, our current findings demonstrate that ectopic expression of T474D induces RPL10 and LIMYB phosphorylation, repressing photosynthesis-related genes and reducing ETR and CO2 assimilation (Figs. 3 and 4). Therefore, any stress signal, including heat and osmotic stress, which activates the NIK1/LIMYB/RPL10 signaling circuit and downregulates translation and photosynthesis-associated marker genes is expected to induce NIK1 phosphorylation at the critical Thr-474 activation site leading to photosynthesis and translation inhibition. This stress-induced coordinated downregulation of translation and photosynthesis-related genes has been extensively demonstrated in genome-wide studies of several plant species. Consistent with our current data, analyses of previously published RNA-seq data in response to heat and osmotic stress in Arabidopsis show that prolonged stress conditions massively downregulate translation-related genes and photosynthesis-associated genes. We propose here that different stress-sensing receptors interact with and activates NIK1 relaying the stress signals to a shared signaling circuit that coordinately downregulates translation and photosynthesis. Therefore, NIK1 functions as a signaling hub for specific stress-sensing receptors.

The TOR signaling rapidly activates translation by phosphorylating regulatory factors in response to stimuli. In contrast, the NIK1 signaling pathway may coordinate the suppression of translation and photosynthesis during stress by regulating the repressive activity of LIMYB, which targets both photosynthesis- and translation-related genes. Thus, NIK1-mediated regulation of photosynthesis and translation represents a delayed response to biotic and abiotic signals, as it depends on the half-life of the target genes. Consistent with this delayed kinetics response, the NIK1 signaling pathway has been shown to suppress global translation after 8 h of NIK1 activation, and photosynthesis repression likely exhibits similar kinetics[15]. However, this delayed response may consist of two distinct phases, as we have shown that the LIMYB-mediated transcriptional repression of target genes leads to decreased protein levels, which precedes the NIK1-mediated suppression of global translation (Fig. 2). These findings support the hypothesis that the NIK1/RPL10/LIMYB signaling module coordinates the negative regulation of both photosynthesis and translation. As a result, the initial reduction in photosynthesis caused by NIK1 activation is driven directly by LIMYB's transcriptional repression of photosynthesis genes rather than the translational control branch of the NIK1 pathway. This coordinated regulation may be essential for balancing carbon supply and demand under stress conditions.

Upon NIK1 activation, LIMYB predominantly targets genes encoding components of the photosynthetic electron transport chain (ETC), photosystem II, and I. Consequently, activation of the NIK1/RPL10/LIMYB module leads to a simultaneous decrease in ETR, gas exchange parameters (A, gs, E, and Ci), fluorescence quantum efficiency, and WUE. These results suggest that the decline in photosynthesis activity displayed by LIMYB-overexpressing lines and T474D lines may result from a reduction in the abundance of Photosystem II, I, ETC components rather than defects in CO_2 fixation or damage to the photosynthetic apparatus. Supporting this hypothesis, we demonstrated that the protein levels of PSI and PSII components were lower in the LIMYB-overexpressing lines compared to the wild-type (Figs. S7 and Table 6). Previous studies have shown that adjustments in the photosystem stoichiometry can impact the quantum efficiency of photosynthesis[20].

However, as stress persists, it is plausible that the NIK1-mediated reduction in global translation will eventually lead to further decreases in photosynthesis at a later stage, affecting not only components and processes in the light reactions but also CO_2 fixation capacity. Two pieces of evidence support this hypothesis. First, we have previously shown that expression of the gain-of-function NIK1-T474D mutant reduces the association of Rubisco mRNA with the polysome fraction[15]. Second, we demonstrate here that LIMYB overexpression leads to a higher reduction in photosynthesis (A) rate than in the PSII electron transport rate (ETR). Defects in CO_2 fixation could then provide feedback to inhibit ETR at the level observed in LIMYB-overexpressing lines, which would, in turn, attenuate the inhibition of CO2 fixation.

A potential pitfall of these studies, however, is the observation that ectopic expression of the constitutively activated NIK1-T474D mutant confers tolerance to drought stress, even though the transgenic lines show reduced photosynthesis, translation, and stunted growth compared to control lines. In most cases, plants respond to low water potential by trying to avoid stress, maintaining the water potential in their tissues close to the unstressed levels[27]. This is typically achieved by balancing the rates of water uptake and loss. In the short term, stomatal dynamics play a significant role in controlling the transpiration rate, consistent with the lower stomatal conductance observed in T474D lines. In the long term, the root-to-shoot ratio is altered, root architecture is modified to maximize water uptake, and shoot growth is reduced[27,28]. There are also modifications in cuticle and lignin thickness affecting water permeability. However, avoiding a decrease in the tissue water potential under water deficit conditions comes at a cost: a reduced photosynthetic rate and reduced productivity if the stress persists[28]. Interestingly, the T474D line displays stunted vegetative growth under normal conditions, which may have primed it for drought tolerance. Indeed, the leaf RWC of these transgenic lines under the water deficit regime remained similar to unstressed conditions, mimicking the plant's stress avoidance mechanism to cope with drought. Additionally, the activation of the NIK1 signaling in the T474D lines may have induced mechanisms of drought tolerance. For instance, ion transporter genes, lignin biosynthetic genes, and genes involved in starvation were enriched in the set of upregulated genes by LIMYB, which requires further investigation.

Our results, along with compelling evidence from the literature, support the argument that NIK1 functions as an influential LRR-RLK information spreader and potentially acts as a coreceptor for various transmembrane stress-sensing receptors (Supplementary Fig. 16). Firstly, we demonstrated that NIK1 undergoes phosphorylation in response to multiple abiotic and biotic signals, activating the NIK1/RPL10/LIMYB signaling circuit, which coordinates the regulation of translation and photosynthesis in plant cells. Conceptually, signaling receptors exhibit high specificity and affinity for stimuli, making it unlikely for a single receptor to be activated by multiple signals. The versability of NIK1 in interacting with different stimulus-specific sensing LRR-RLKs, forming a hub with high centrality, supports the notion that NIK1 can transduces different stress signals as a coreceptor[17–19]. Furthermore, NIK1 belongs to the LRRII subfamily of RLKs and shares similar structural and biochemical properties with BAK1, the almost universal coreceptor for LRR-RLKs/RLPs[19,29]. Notably, the extracellular domain (ECD) of BAK1, crucial for assembling the correct receptor/coreceptor pair, is structurally equivalent to the NIK1 ECD[30]. Finally, we have shown that NIK1 relays information from the immune complex FLS2-BAK1, transmitting biotic signals that culminate in the coordinate regulation of translation- and photosynthesis-related genes[17] (and this work). The bacterial PAMP flg22, but not viral PAMPs, requires the immune complex FLS2-BAK1 for mediating NIK1 phosphorylation and activation. Hence, it is plausible that a yet-to-be-determined viral pattern recognition receptor might be responsible for sensing viral PAMPs and mediating NIK1 activation during viral infection. Similarly, NIK1

may transduce different abiotic signals by relaying information from other specific stress-sensing receptors. Based on these findings, we propose that NIK1 functions as a central signaling hub, integrating signals from multiple stress-sensing receptors to regulate growth under stressful conditions.

Methods

Plant material and growth conditions

The *Arabidopsis thaliana* ecotype Columbia-0 (Col-0) was used as control lines. The knockout lines *nik1-1* (SALK_060808), *nik2-1* (SALK_044363), *fls2* (Salk_141277), *bak1-4* (Salk_116202), and *limyb-32* (SALK_032054) were obtained from the Arabidopsis Biological Resource Center and have been previously characterized[10,15,31]. The double mutant *nik1-1/nik2*, the transgenic line RPL10-1, harboring the construct 35S: YFP-GR-RPL10 in the Col-0 genetic background, two independently *nik1-1* transformed lines, T474D-4, T474D-6, expressing the NIK1-T474D-GFP mutant transgene, the NIK1-HA transgenic line, harboring 35S:NIK1-HA in Col-0 and the *limyb*/T474D-2 line expressing 35S:T474D-GFP in the *limyb-32* mutant background have been generated previously[15,17]. Plants were grown in soil (Metro Mix 366) in a growth chamber at 23 °C, 45% humidity, and 75 μE/m^2/s^1 light with a 10-h-light/14-h-dark photoperiod. Four-week-old plants were used for treatments with viral nucleic acid elicitors, heat stress, and protoplast isolation. For osmotic stress experiments, seedlings were germinated for up to 12 days on half-strength Murashige and Skoog ($MS^1/_2$) plates containing 1% (w/v) sucrose and 0.8% (w/v) agar, grown under the same conditions.

Plasmid construct for transient expression in protoplast

The generation of pK7F-NIK1T474D (pUFV632), which expresses a T474D mutant fused in frame with the N-terminal of GFP under the control of CaMV 35S promoter, has been previously described[12]. The clones pK7F-L10 (pUFV1862) and pYFP-L10 (pUFV2365) have been previously described[12]. They contain RPL10A ORF fused in frame to GFP after its last codon or YFP before its first codon under the control of the 35S promoter. The recombinant plasmid pYFP-LIMYB (pUFV1886), containing LIMYB ORF fused in-frame to the C-terminus of YFP under the control of the 35S promoter and inserted into the binary vector 35S-YFP-casseteA-Nos-pCAMBIA1300, and the recombinant plasmid AT5G05800NS-pK7FWG2 (pUVF1395), containing LIMYB ORF fused-in frame to the N-terminal of GFP under control of the 35S promoter, have been described before[15].

Whole-genome chromatin immunoprecipitation sequencing (ChIP-Seq) and data analysis

Seedlings (600 mg) harboring a YFP-LIMYB transgene were crosslinked using 1% formaldehyde in PBS solution (Sigma-Aldrich, cat. # F8775) under vacuum for 1-3 min, as previously described[32]. After nuclei isolation, chromatin was sonicated up to 100–800 bp fragments. LIMYB-GFP targets from LIMYB-32-L1-, LIMYB-32-L3-, and LIMYB-32-L4-isolated nuclei were immunoprecipitated using rabbit polyclonal anti-GFP - IgG antibody (Thermo Fisher Scientific, MA, USA, cat. # A11122, 1:5,000) and captured with protein-A agarose beads (Invitrogen™, Cat # 15918014). After elution, reverse crosslinking and DNA purification, ChIPed-DNA was used to generate sequencing libraries through the Illumina TruSeq kit (Illumina, cat # IP-202-1012, IP-202-1014) according to the manufacturer's protocols. Libraries were sequenced using an Illumina HiSeq 4000. The quality of the reads was evaluated through the statistical metrics implemented in the FastQC data quality analysis tool (https://www.bioinformatics.babraham.ac.uk/projects/fastqc); low-quality sequencing reads were filtered using the printSEQ software package[33]. ChIP-Seq raw reads were aligned to the TAIR10 genome sequence using Bowtie 2[34]. ChIP-seq peaks were calculated with the software ChIPpeakAnno[35,36], and MACS2[37] was used to analyze the ChIP-seq data. Putative target genes and peak distribution of the ChIP-seq data were figured out using the ChIPpeakAnno software[35,36]. Motif discovery was performed by Multiple EM for Motif Elicitation (MEME) program (http://meme.nbcr.net/meme/), MEME-ChIP version 4.9.0. Motifs were grouped by applying hierarchical clustering using motif distances, calculated by Pearson correlated coefficients as the metric for base comparison, and the Smith-Waterman Ungapped alignment method[38]. The binding intensity was measured from log2 (normalized counts of reads/peaks) and evaluated at E-value cut-off of 1e-05 for sequence identification. ChIP-seq data have been deposited in the Gene Expression Omnibus under accession number GSE197332.

RNA-sequencing (RNA-seq) method and data analysis

For RNA-seq experiments, we used three biological replicates of a pool of 12-day-old Col-0, *LIMYB-32-L1*, and *LIMYB-32-L3* seedlings and examined differences between Col-0 and LIMYB lines using the Deseq2 differential gene expression method[39,40]. RNA sequencing was obtained using the Illumina Hi-seq 2500 platform. Libraries for RNA-seq were prepared with the TrueSeq-RNA Sample Prep Illumina kit (Illumina, cat # 20020595). The paired-end 100-bp protocol was used with the following quality filter parameters: 5 bases trimmed at the 3′ and 5′ ends of the reads and a minimum average Phred score of 30. Reads quality was evaluated by FastQC (https://www.bioinformatics.babraham.ac.uk/projects/fastqc). Illumina adapters were removed using Trimmomatic software[41], and low-quality sequencing reads were filtered and trimmed using prinSEQ software package[33]. Read mapping was performed using the Bowtie 2 program[34]. The global analysis of differential gene expression (DGE) was performed using the edger package[34] and DEseq2[39]. Differential expression was determined using the *p*-value adjusted by the "False discover rate" (FDR). Log_2.Fold Change *p*-value < 0.01 e log2-fold-change > 1.0 for upregulated genes and log2-fold-change < 1.0 for downregulated genes were used as the cut-off point. Differentially expressed (DE) genes were stored using SQL tables in the PostgreSQL relational database (http://inctipp.bioagro.ufv.br/, http://200.235.143.46/LiMyb/ or https://inctipp.bioagro.ufv.br/maloni/), which listed corresponding log2 FC (fold change) and *p* values corrected by false discovery rate (q value) for all DE genes. The classification of gene ontology (GO) and analysis of enrichment of pathways were performed using the packages GoStats[42] and PathView[43], both present in the R/Bioconductor GOstats repository. The significant *p*-value for enrichment was $p < 0.01$.

Activation of the NIK1 pathway by begomovirus-derived nucleic acids and flg22

Leaf discs from transgenic lines previously injured with an abrasive were excised by a cork borer and incubated overnight in 12-well plates containing 500 μL ultra-pure water. Then the water was immediately replaced with 500 μL TE buffer supplemented with 250 ng/μL of viral nucleic acids (DNA or total RNA prepared from begomovirus-infected plants and treated with proteases, Rnase, or DNase), 100 mM flg22 or ultra-pure water. NIK1 activation was monitored by phosphorylation at 10 to 60 min after treatment. Phosphorylation of RPL10 was examined at 30 min to 3 h post-treatment, whereas the transcript accumulation of target genes was measured at a minimum of 3 h after treatment.

Protoplast preparation from *A. thaliana* leaves

Expanded leaves from 3–4-week-old plants were cut into 0.5–1-mm pieces and digested with 5–10 ml enzyme solution (20 mM MES pH 5.7; 1.5% cellulase R10; 0.4% macerozyme R10; 0.4 M mannitol and 20 mM KCl). The leaf strips were vacuum infiltrated for 30 min in the dark using a desiccator. Then, the digestion was conducted without shaking in the dark for at least 3-h at room temperature. The integrity of the protoplasts was examined under a light microscope. The protoplasts were filtered to remove undigested leaf tissues and recovered by centrifugation. The protoplasts were transformed using the protocol of DNA-PEG–calcium transfection, in which 10 μl DNA (10–20 μg of plasmid DNA) were mixed

with 2×10^4 protoplasts along with 5% PEG solution (Polyethylene glycol 4000, sigma, Cat # 25322-68-3) at room temperature for up to 15 min and then incubated for recovery during 12 h[44].

Electrophoretic mobility shift assay (EMSA)

For EMSA, the His-tagged LIMYB was affinity-purified from the IPTG-induced E. coli protein soluble fraction using Ni-NTA agarose (Quiagen®), according to the manufacturer's recommendations, and resolved by SDS-PAGE. Synthetic oligonucleotídeos (5′-GATGGA GGAAG**CAAAA-C**ATTGACCAT-3′ and 5′-ATGGTCAAT**GTTTTG**CTTCCTCCATC-3′) from RPL18 promoter containing the putative CAAAAC DNA binding site were annealed and the dsDNA was biotinylated using the 3′ OH biotin labeling kit from Pierce (Pierce™ Biotin 3′-end DNA labeling kit, catalog number 89818). EMSAs were performed using a Light Shift Chemiluminescent EMSA kit (Thermo Scientific), according to the manufacturer's instructions. A 100-fold molar excess of the RPL18 unlabeled 26-pb dsDNA fragment was used as specific competitor (5′-ATGGTCAAT**CAC-GAT**CTTCCTCCATC-3′). For non-specific competitor, the DNA binding site from the RPL18 fragment was replaced by ATCGTG (5′-GATGGAG-GAAG**ATCGTG**ATTGACCAT-3′).

Phosphorylation assay

Protoplasts of *nik1-1, nik2-1, fls2, bak1-4*, and *nik1-1/nik2-1* mutant lines were transformed with RPL10-GFP. After 16-h incubation for transient transgene expression, the protoplasts were treated with nucleic acids prepared from mock-inoculated and begomovirus-infected plants or 100 mM flg22 for 3-h. RPL10-GFP was immunoprecipitated with α-GFP antibodies and protein-A agarose beads, fractionated by SDS-PAGE, and immunoblotted with an α-phosphoserine antibody (α-phosphoserine peroxidase, Sigma-Aldrich, Cat # SAB5200087, 1:5000) and an α-GFP antibody (α -GFP, life technologies, cat # A11122, 1:5000; goat anti-mouse IgG-HRP, Santa Cruz, Cat # sc-2005, 1:10,000). Likewise, RPL10-GFP- and NIK1-HA-expressing transgenic lines were treated for 3-h with nucleic acids prepared from uninfected and begomovirus-infected plants or 100 mM flg22. Then, RPL10-GFP and NIK1-HA were immunoprecipitated from leaf discs from treated and non-treated plants with an α-GFP antibody or α-HA antibodies (α-HA, Thermo Fisher, Cat # 71-5500, 1:50) and protein-A agarose beads (InvitrogenTM, Cat # 15918014), fractionated by SDS-PAGE and immunoblotted with an α-phosphoserine antibody (α-phosphoserine peroxidase, Sigma-Aldrich, Cat # SAB5200087, 1:5000) or α-phosphothreonine antibody (α-phosphothreonine, Thermo Fisher, Cat # 71-8200, 1:250) and goat anti-rabbit IgG secondary antibody (Thermo Fisher, Cat # 65-6120, 1:10.000). The same protocol examined the heat and osmotic-induced phosphorylation of NIK1-HA and RPL10 in 22-day-old transgenic lines.

RNA isolation and RT-qPCR analysis

For RNA isolation, either 12-day-old seedlings grown on half-strength MS plates or leaf discs of 22-day-old plants were transferred to 1 mL H_2O in a 12-well plate to recover overnight and then treated with uninfected and begomovirus-infected nucleic acid preparation or 100 nM flg22 for 15 min to 3 h, or 10% PEG 8000 for 3-h and 24-h. RNA was extracted using TRIzol reagent (Invitrogen™, cat # 15596018, USA) and quantified with a NanoSpec spectrophotometer. Total RNA was treated with DNase I, RNase-free (Thermo Scientific™, cat # EN052) for 30 min at 37 °C and then reversed transcribed with M-MLV Reverse Transcriptase (Invitrogen™, cat # 28025013). Real-time PCR was performed using iTaq Universal SYBR Green Supermix (Bio-Rad, cat # 1725121, USA) and a 7500 Fast Real-Time PCR System (Applied Biosystems™, cat # 4351106, USA). The expression of each gene was normalized to the expression of Actin or UBQ10. The primers used to analyze specific transcripts for RT-qPCR are listed in Supplementary Table 8.

Promoter transactivation assay in protoplasts and *Nicotiana benthamiana* leaves

The protoplasts were isolated from Col-0 and *limyb-32*, and co-transformed with the combinations: pK7F-NIK1T474D + proL18(2):Lucif-term-2X35S:RLucifpH7M34GW (−2000 bp); pK7F-NIK1T474D + AT5G0 5800NS-pK7FWG2 + proL18(2):Lucif-term-2X35S:RLucifpH7M34GW; AT 5G05800NS-pK7FWG2 + proL18(2):Lucif-term-2X35S:RLucifpH7M34 GW; pK7F-NIK1T474D + proUBQ:Lucif-term-2X35S:RLucifpH7M34GW; pK7F-NIK1T474D + AT5G05800NS-pK7FWG2 + proUBQ:Lucif-term-2X3 5S:RLucifpH7M34GW.

N. benthamiana leaves were agroinfiltrated with *A. tumefaciens* GV3101 strains carrying the following combinations in the absence and presence of LIMYB cDNA (AT5G05800NS-pK7FWG2): proPH-SIIOEC:Lucif-term-2X35S:RLucifpH7M34GW (-2000 bp), proFD1:Lu-cif-term-2X35S:RLucif pH7M34GW (−2000 bp); proL18Ae(1):Lucif-term-2 × 35S:RLucif pH7M34GW (−1000 bp); proL18(3):Lucif-term-2X35S:RLucif pH7M34GW (−400 bp), proUBQ:Lucif-term-2X35S:RLucifpH7M34GW. Forty-eight hours after infiltration, 200 mg of leaf tissue were harvested for total protein extraction. Luciferase activity was assayed with Dual-Luciferase® Reporter Assay System (Promega, cat # E1910) according to the manufacturer's instructions.

Photosynthetic and photochemical analysis of LIMYB and T474D overexpressing lines

Gas exchange and chlorophyll fluorescence measurements were carried out in expanded leaves from 30-day-old LIMYB and T474D lines, grown in a chamber at 23°C. Gas exchange rates were determined in the morning, applying different photon rates $m^{-2}s^{-1}$ for photosynthetic efficiency analysis, using an infrared gas concentration determination system (IRGA, LCpro-SD - ®ADC Bio scientific, Hoddesdon, England). The net assimilation of carbon (A, μmol CO_2 m -2 s -1), stomatal conductance (gs, mol H_2O m-2s -1), the internal concentration of CO_2 (Ci, μmol CO_2 mol -1), transpiration rate (E, mmol m-2 s-1) and water-use efficiency (WUE, A/E μmol m-2 s-1/mmol H2O m-2 s-1), under CO_2 concentrations controlled by the use of a gas cylinder attached to the equipment. Photochemical parameters of PSII and the energy transmission of the light-capturing complex (Lchb) were determined with a modulated light fluorometer (MINI-PAM, Walz, Effeltrich, Germany). Minimum (Fo) and maximum (Fm) fluorescence of dark-adapted leaves were also determined in the morning to analyze PSII Effective quantum yield (YII) and electron transport rate (ETR = ΦPSII x PAR x 0,5 × 0,84, where the ETR factor has been assumed to be that of a model leaf, with 50 % of the PAR (photosynthetically active radiation) being distributed to PSII and 84% of the PAR being absorbed by photosynthetic pigments in a standard leaf)[45]. ETR rate was determined via modulated light pulse, the response curve of chlorophyll-a fluorescence parameters (ETR, ΦPSII, ΦNO, and qL) in responses to eight increasing light levels based on Fo and Fm values (minimum value up to the saturating pulse).

Heat stress

The heat stress treatment was performed as described[46,47], with some modifications. Twenty-eight-day-old plants were subjected to 27 °C or 38 °C for 0 to 3-h. NIK1 phosphorylation was monitored 0, 10, 15, 20, 30, and 60 min post-treatment. As for RPL10 phosphorylation and transcript accumulation of target genes, 0, 1-h, and 3-h were taken after treatment. After the specified treatment period, the leaves were immediately frozen in liquid nitrogen for protein and/or total RNA extraction.

Osmotic stress

Osmotic stress was induced in Arabidopsis seedlings as described[48], with some modifications. 12-days-old *Arabidopsis thaliana* seedlings

were germinated on Murashige and Skoog (MS) medium containing 1% sucrose (pH 5.7) in a petri dish and then placed in 12-well plates containing 90% liquid MS medium (1/4 strength) and 10% polyethylene glycol (PEG, MW 8000, SIGMA, cat # 25322-68-3) (p/v) for 3- and 24-h.

Protein extraction and proteomic analysis

Protein was extracted from five pools of nine-day-old Arabidopsis seedlings (biological replicates) of Col-0 control lines and three LIMYB-32-overexpressing lines (L1, L3, L4), totaling 20 samples. Seeds were germinated on ½-strength MS medium plates. Protein extraction followed Song et al.[49] with modifications: 250 mg of plant material was ground in liquid nitrogen using a pre-cooled mortar and pestle, then homogenized in lysis buffer (8 M urea, 100 mM Tris pH 7, 20 mM DTT, ½ × EDTA-free protease inhibitor cocktail [Roche]) at a 1:1 (w/v) ratio. Homogenization was completed using a TissueLyser II (QIAGEN, Hilden, Germany; 30 Hz, 3 min) followed by centrifugation (4000 × *g*, 3 min), repeated three times. Proteins were acetone-precipitated (4 volumes ice-cold acetone, −20°C, 30 min), pelleted (4500 × *g*, 10 min, 4°C), washed with 80% acetone (sonicated 5 min, bath sonicator), and centrifuged again (repeated three times). Pellets were resuspended in 8 M urea/50 mM Tris pH 7.5/20 mM DTT (100 μL final volume). Protein concentration was determined by Bradford assay (Thermo Fisher Scientific, Waltham, MA, USA). For short-run gels and protein identification, extracted proteins (40 μg/lane) were separated on 10% polyacrylamide gels (1.5 mm thick, 1.5 M Tris-HCl pH 8.8) using Laemmli buffer[50] (277.8 mM Tris-HCl pH 6.8, 44.4% glycerol, 4.4% SDS) at 200 V until proteins migrated 1.0 cm into the gel. Gels were fixed (10% methanol/5% acetic acid, 2 h), stained with Coomassie G250 (48 h), and excised bands were destained (50 mM NH_4HCO_3/50% methanol), reduced (200 mM DTT, 56°C, 30 min), alkylated (200 mM iodoacetamide, RT, 30 min), and digested with trypsin (37°C, 20 h). Peptides were extracted (50% acetonitrile/5% formic acid), desalted (C18 ZipTips; Merck Millipore, Burlington, MA, USA), and dissolved in 20 μL 0.1% formic acid. LC-MS/MS analysis was performed on a nanoAcquity UPLC system (Waters, Milford, MA, USA) coupled to a Q-ToF MAXIS 3 G (Bruker Daltonics, Billerica, MA, USA). Peptides were trapped (nanoAcquity UPLC 2G-V/MTrap, 5 μm Symmetry C18, 180 μm × 20 mm) and separated (nanoAcquity UPLC BEH130 C18, 1.7 μm, 100 μm × 100 mm) at 0.3 μL/min with a 320-min gradient (0.1% formic acid in water/acetonitrile). The solvent system consisted of (A) 0.1% formic acid in water and (B) 0.1% formic acid in acetonitrile, with a gradient as follows: 0/2% B; 1/2% B; 300/30% B; 305/85% B; 310/85% B; 315/2% B; and 320/2% B. NanoESI ionization (CaptiveSpray; 2.0 kV, 150°C, 3 L/min dry gas) was used with positive-mode scanning (300–1500 m/z). Data were acquired in data-dependent acquisition (DDA) mode, with the 20 most intense precursors selected for fragmentation per cycle. Data were acquired using HyStar (Bruker) and processed with DataAnalysis (Bruker) and PEAKS 9.0 (Arabidopsis UniProt database; FDR < 1%, ≥3 unique peptides; variable oxidation, fixed carbamidomethylation; 20 ppm mass error).

Bioinformatics analysis of the proteomic data

Proteomics raw data obtained using the PEAKS software were imported into Perseus version 2.1.3.0[51]. The input file initially contained 1854 identified proteins. To ensure the quality and reliability of the analysis, filtering was applied to retain only proteins with at least three valid values per treatment among the experimental samples. After applying this criterion, 525 proteins were selected for subsequent analyses. Missing values were imputed based on a simulated normal distribution using Perseus' default parameters. This approach minimizes bias and ensures robustness for subsequent statistical analyses, enabling reliable and replicable results. The data processed in Perseus were then exported and analyzed using MetaboAnalyst 6.0[52]. The first step involved applying variance filtering based on the standard deviation, using a cutoff threshold of 25%. Next, an abundance filter based on mean intensity values was applied to remove proteins with consistently low levels, prioritizing the most informative proteins. To ensure comparability among the samples, the data were normalized using the median method and scaled using Pareto scaling. Differential protein abundance analysis was conducted based on the $\log_2$ intensity of the peaks. In this step, three biological replicates from each treatment group (LIMYB-L1, LIMYB-L3, and LIMYB-L4) were evaluated against the control group (Col-0). Replicates were selected based on their highest grouping in a principal component analysis (PCA). Differentially expressed proteins among the experimental groups were identified with a statistical significance threshold of $p < 0.01$ and $-1 <$ log2 peak intensity > 1. This statistical analysis enabled the identification of proteins with significant changes.

Statistical analysis

A two-tailed unpaired Student's *t*-test and was used for statistical analysis to compare two groups. One-way analysis of variance (ANOVA), followed by Dunnett's post hoc test, was used for multiple comparisons and comparisons with the control group. Unless specifically stated, the analyses were executed with three-independent experiments, and the data were expressed as means ± SE. A significant difference was considered *p*-value ≤ 0.05. The photosynthetic parameters analysis used 3° order polynomial regression on adjusted radiation curves and Student's *t*-test to compare curvature points.

Reporting summary

Further information on research design is available in the Nature Portfolio Reporting Summary linked to this article.

Data availability

The authors declare that the data supporting the findings of this study are available in the main text and in Supplementary Information files. The source data underlying Figs. 1c–h, 2a–h, 3a–c, 4a–h, 5a–f, 6a–g, 7a–i, 8a–f and Supplementary Figs. S1a, b–d–f, S2a–e, S3b, c, S4a–c, S6a–e, S7a–f, S8b–g, S9b–f, S10a–d, S12a–e, S13b–e, S14a–c, S15b, c are provided as Source Data file. The ChIP-seq data generated in this study have been deposited in the Gene Expression Omnibus under accession number GSE197332. The RNA-seq data used in this study have been deposited in the Gene Expression Omnibus under accession GSE294149. The mass spectrometry proteomics data generated in this study have been deposited in the MassIVE repository under the identifier MSV000097120 [https://massive.ucsd.edu/ProteoSAFe/dataset.jsp?task=1720848d46cf4cf0aba6fac809df5daa] and registered with the ProteomeXchange Consortium under the identifier PXD060833 Source data are provided with this paper.

References

1. Muhammad, I. et al. Mechanisms regulating the dynamics of photosynthesis under abiotic stresses. *Front. Plant Sci.* **11**, 615942 (2021).
2. Reinbothe, C., Pollmann, S. & Reinbothe, S. Singlet oxygen signalling links photosynthesis to translation and plant growth. *Trends Plant Sci.* **15**, 499–506 (2010).
3. Song, Y. et al. Function of chloroplasts in plant stress responses. *Int. J. Mol. Sci.* **22**, 13464 (2021).
4. Tcherkez, G. et al. Protein synthesis increases with photosynthesis via the stimulation of translation initiation. *Plant Sci.* **291**, 110352 (2020).
5. Ferreira, M. A., Teixeira, R. M. & Fontes, E. P. B. Geminivirus–host interactions: action and reaction in receptor-mediated antiviral immunity. *Viruses* **13**, 840 (2021).
6. Fontes, E. P. B., Teixeira, R. M. & Lozano-Durán, R. Plant virus-interactions: unraveling novel defense mechanisms under immune-suppressing pressure. *Curr. Opin. Biotechnol.* **70**, 108–114 (2021).

7. Machado, J. P., Brustolini, O. J., Mendes, G. C., Santos, A. A. & Fontes, E. P. B. NIK1, a host factor specialized in antiviral defense or a novel general regulator of plant immunity? *Bioessays* **37**, 1236–1242 (2015).
8. Machado, J. P. B., Calil, I. P., Santos, A. A. & Fontes, E. P. B. Translational control in plant antiviral immunity. *Genet. Mol. Biol.* **40**, 292–304 (2017).
9. Teixeira, R. M., Ferreira, M. A., Raimundo, G. A. S. & Fontes, E. P. B. Geminiviral triggers and suppressors of plant antiviral immunity. *Microorganisms* **9**, 775 (2021).
10. Fontes, E. P. B., Santos, A. A., Luz, D. F., Waclawovsky, A. J. & Chory, J. The geminivirus nuclear shuttle protein is a virulence factor that suppresses transmembrane receptor kinase activity. *Gene Dev.* **18**, 2545–2556 (2004).
11. Mariano, A. C. et al. Identification of a novel receptor-like protein kinase that interacts with a geminivirus nuclear shuttle protein. *Virol* **318**, 24–31 (2004).
12. Santos, A. A., Carvalho, C. M., Florentino, L. H., Ramos, H. J. & Fontes, E. P. B. Conserved threonine residues within the A-loop of the receptor NIK differentially regulate the kinase function required for antiviral signaling. *PLoS One* **4**, e5781 (2009).
13. Teixeira, R. M. et al. Virus perception at the cell surface: revisiting the roles of receptor-like kinases as viral pattern recognition receptors. *Mol. Plant Pathol.* **20**, 1196–1202 (2019).
14. Carvalho, C. M. et al. Regulated nuclear trafficking of rpL10A mediated by NIK1 represents a defense strategy of plant cells against virus. *PLoS Pathog.* **4**, e1000247 (2008).
15. Zorzatto, C. et al. NIK1-mediated translation suppression functions as a plant antiviral immunity mechanism. *Nature* **520**, 679–682 (2015).
16. Brustolini, O. et al. Sustained NIK-mediated antiviral signalling confers br-spectrum tolerance to begomoviruses in cultivated plants. *Plant Biotechnol. J.* **13**, 1300–1311 (2015).
17. Li, B. et al. The receptor-like kinase NIK1 targets FLS2/BAK1 immune complex and inversely modulates antiviral and antibacterial immunity. *Nat. Commun.* **10**, 4996 (2019).
18. Ahmed, H. et al. Network biology discovers pathogen contact points in host protein-protein interactomes. *Nat. Commun.* **9**, 673–681 (2018).
19. Smakowska-Luzan, E. et al. An extracellular network of Arabidopsis leucine-rich repeat receptor kinases. *Nature* **553**, 342–346 (2018).
20. Chow, W. S., Melis, A. & Anderson, J. M. Adjustments of photosystem stoichiometry in chloroplasts improve the quantum efficiency of photosynthesis. *Proc. Natl. Acad. Sci. USA* **87**, 7502–7506 (1990).
21. Chong, G. L., Foo, M. H., Lin, W.-D., Wonga, M. M. & Versluesa, P. E. Highly ABA-Induced 1 (HAI1)-Interacting protein HIN1 and drought acclimation-enhanced splicing efficiency at intron retention sites. *Proc. Natl. Acad. Sci. USA* **116**, 22376–22385 (2019).
22. Watkins, J. M. et al. Phosphorylation dynamics in a flg22-induced, heterotrimeric G-protein dependent signaling network in Arabidopsis thaliana reveals a candidate PP2A phosphatase involved in AtRGS1 trafficking. *Mol. Cell Proteom.* **23**, 100705 (2024).
23. Fontes, E. P. B. SERKs and NIKs: coreceptors or signaling hubs in a complex crosstalk between growth and defense? *Curr. Opin. Plant Biol.* **77**, 102447 (2024).
24. Hosseini, S., Schmidt, E. D. L. & Bakker, F. T. Leucine-rich repeat receptor-like kinase II phylogenetics reveals five main clades throughout the plant kingdom. *Plant J.* **103**, 547–560 (2020).
25. Santos, A. A., Lopes, K. V. G., Apfata, J. A. C. & Fontes, E. P. B. NSP-interacting kinase, NIK: a transducer of plant defence signalling. *J. Exp. Bot.* **61**, 839–3845 (2010).
26. Yan, L. et al. Structural basis for the impact of phosphorylation on the activation of plant receptor-like kinase BAK1. *Cell Res* **22**, 1304–1308 (2012).
27. Seleiman, M. F. et al. Drought stress impacts on plants and different approaches to alleviate its adverse effects. *Plants* **10**, 259 (2021).
28. Yang, X. et al. Response mechanism of plants to drought stress. *Horticulturae* **7**, 50 (2021).
29. Sakamoto, T. et al. The tomato RLK superfamily: phylogeny and functional predictions about the role of the LRRII-RLK subfamily in antiviral defense. *BMC Plant Biol.* **12**, 229 (2012).
30. Jaillais, Y., Belkhadir, Y., Balsemão-Pires, E., Dangl, J. L. & Chory, J. Extracellular leucine-rich repeats as a platform for receptor/coreceptor complex formation. *Proc. Natl Acad. Sci. USA* **108**, 8503–8507 (2011).
31. Li, B. et al. Phosphorylation of trihelix transcriptional repressor ASR3 by MAP KINASE4 negatively regulates Arabidopsis immunity. *Plant Cell* **27**, 839–856 (2015).
32. Yamaguchi, N. et al. PROTOCOLS: Chromatin Immunoprecipitation from Arabidopsis Tissues. *Arabidopsis Book* **12**, e0170 (2014).
33. Schmieder, R. & Edwards, R. Quality control and preprocessing of metagenomic datasets. *Bioinformatics* **27**, 863–864 (2011).
34. Langmead, B., Trapnell, C., Pop, M. & Salzberg, S. L. Ultrafast and memory-efficient alignment of short DNA sequences to the human genome. *Genome Biol.* **10**, R25 (2009).
35. Zhu, L. J. et al. *Integrative Analysis of ChIP-Chip and ChIP-Seq Dataset*. In: Lee, T. L., Shui Luk, A. (eds) Tiling Arrays. *Methods in Mol. Biol.* **1067**, (Humana Press, 2013).
36. Zhu, L. J. et al. ChIPpeakAnno: a bioconductor package to annotate ChIP-seq and ChIP-chip data. *BMC Bioinforma.* **11**, 237 (2010).
37. Zhang, Y. et al. Model-based analysis of ChIP-Seq (MACS). *Genome Biol.* **9**, R137 (2008).
38. Song, L. et al. A transcription factor hierarchy defines an environmental stress response network. *Science* **354**, aag1550 (2016).
39. Anders, S. & Huber, W. Differential expression analysis for sequence count data. *Genome Biol.* **11**, R106 (2010).
40. Robinson, M. D. & Oshlack, A. A scaling normalization method for differential expression analysis of RNA-seq data. *Genome Biol.* **11**, 3–25 (2010).
41. Bolger, A. M., Lohse, M. & Usadel, B. Trimmomatic: a flexible trimmer for Illumina sequence data. *Bioinformatics* **30**, 2114–2120 (2014).
42. Falcon, S. & Gentleman, R. Using GOstats to test gene lists for GO term association. *Bioinformatics* **23**, 257–258 (2007).
43. Luo, W. & Brouwer, C. Pathview: an R/bioconductor package for pathway-based data integration and visualization. *Bioinformatics* **29**, 1830–1831 (2013).
44. Yoo, S. D., Cho, Y. H. & Sheen, J. Arabidopsis mesophyll protoplasts: a versatile cell system for transient gene expression analysis. *Nat. Protoc.* **2**, 1565–1572 (2007).
45. Schreiber, U., Klughammer, C. & Kolbowski, J. Assessment of wavelength-dependent parameters of photosynthetic electron transport with a new type of multi-color PAM chlorophyll fluorometer. *Photosynth. Res.* **113**, 127–144 (2012).
46. Chao, L. M., Liu, Y.-Q., Che, D.-Y., Xue, X.-Y. & Mao, Y.-B. *Arabidopsis* transcription factors *SPL1* and *SPL12* confer plant thermotolerance at reproductive stage. *Mol. Plant* **10**, 735–748 (2017).
47. Wang, L. et al. Differential physiological, transcriptomic and metabolomic responses of Arabidopsis leaves under prolonged warming and heat shock. *BMC Plant Biol.* **20**, 86 (2020).
48. Costa, M. D. L. et al. A new branch of endoplasmic reticulum stress signaling and the osmotic signal converge on plant-specific asparagine-rich proteins to promote cell death. *J. Biol. Chem.* **283**, 20209–20219 (2008).
49. Song, G. et al. Heterotrimeric G-protein-dependent proteome and phosphoproteome in unstimulated Arabidopsis roots. *Proteomics* **18**, 1800323 (2018).

50. Laemmli, U. K. Cleavage of structural proteins during the assembly of the head of bacteriophage T4. *Nature* **227**, 680–685 (1970).
51. Tyanova, S. & Cox, J. Perseus: a bioinformatics platform for integrative analysis of proteomics data in cancer research. *Methods Mol. Biol.* **1711**, 133–148 (2018).
52. Pang, Z. et al. MetaboAnalyst 6.0: towards a unified platform for metabolomics data processing, analysis and interpretation. *Nucleic Acids Res.* **52**, W398–W406 (2024).

Acknowledgements

This research was supported by Conselho Nacional de Desenvolvimento Científico e Tecnológico (CNPq Grant 406440/2022-0 to E.P.B.F.) and Fundação de Amparo à Pesquisa do Estado de Minas Gerais, Brazil (Fapemig Grant RED-00205-22, BPD-00911-22, APQ-03607-23 to E.P.B.F, APQ-04824-24 to C.E.M.D., APQ-01357-22 to P.A.B.R.). M.A.F. is a pos-doctor fellow from Fapemig/CNPq Profix. R.M.T. was supported by a graduate fellowship from Fapemig. T.F.F.S., N.G.A.R. are recipients of CAPES graduate fellowships. S.S.B. and F.R.S. are recipient of CNPq graduate fellowships. E.G.D.S. is a pos-doctoral fellow from Fapemig. C.E.M.D. was a pos-doctoral fellow from Capes.

Author contributions

M.A.F., R.M.T., and E.P.B.F. conceived the project, designed experiments, and analyzed data. M.A.F. and R.M.T. performed the NIK1 and RPL10 phosphorylation assays, viral PAMP assays, heat stress experiments, and examined the readouts of the pathway. M.A.F. conducted the osmotic stress experiments. O.J.B.B. and E.G.D.S. performed the bioinformatics analysis and the statistical analysis of the data. T.F.F.S. and J.J.-B. Generated LIMYB mutants and performed LIMYB phosphorylation and RT-qPCR of target genes. N.G.A.R. purified LIMYB, performed EMSA, and assisted in heat stress assays. S.S.B. performed the transactivation assays and assisted in protein phosphorylation assays. F.R.S. and C.C.O. performed the in silico resolution of the LIMYB 3D model. F.R.S. and M.A.F. performed the proteomic analysis. B.A.L. C.E.M.D. purified proteins and prepared antibodies. L.L.L. and B.A.L. conducted the photosynthesis assays, analyzed data, and growth parameters. L.L.O. assisted in the generation of antibodies. H.J.O.R. and P.A.B.R. analyzed data and provided critical feedback. M.A.F. and E.P.F.B. wrote the manuscript with inputs from all co-authors.

Competing interests

The authors declare no competing interests.

Additional information

Supplementary information The online version contains supplementary material available at https://doi.org/10.1038/s41467-025-59571-y.

Correspondence and requests for materials should be addressed to Marco Aurélio Ferreira or Elizabeth P. B. Fontes.

Peer review information *Nature Communications* thanks the anonymous reviewers for their contribution to the peer review of this work. A peer review file is available.

[1]Department of Biochemistry and Molecular Biology, Universidade Federal de Viçosa, Viçosa, Minas Gerais, Brazil. [2]National Institute of Science and Technology in Plant-Pest Interactions, Bioagro, Universidade Federal de Viçosa, Viçosa, Minas Gerais, Brazil. [3]National Laboratory for Scientific Computing (LNCC), Petrópolis, RJ, Brazil. [4]Brazilian Bioenewables National Laboratory (LNBR), Brazilian Center for Research in Energy and Materials (CNPEM), Campinas, Brazil. [5]Laboratório de Investigação Biológica, Department of Biomedical Sciences and Health, Universidade do Estado de Minas Gerais, Passos, Brazil. [6]Department of General Biology, Universidade Federal de Viçosa, Viçosa, Minas Gerais, Brazil. [7]These authors contributed equally: Marco Aurélio Ferreira, Ruan M. Teixeira. ✉e-mail: marco.a.ferreira@ufv.br; bbfontes@ufv.br